

# How to identify the dead cone in the top-quark jet

Stefan Kluth and Wolfgang Ochs

*Max-Planck-Institut für Physik, Boltzmannstr. 8, 85748 Garching, Germany*

Redamy Perez-Ramos

*DRII-IPSA, Bis, 63 Boulevard de Brandebourg, 94200 Ivry-sur-Seine, France,  
Laboratoire de Physique Théorique et Hautes Energies (LPTHE), UMR 7589,  
Sorbonne Université et CNRS, 4 place Jussieu, 75252 Paris Cedex 05, France*

The gluon emission from an energetic heavy quark is suppressed in the forward direction below the angle  $\Theta \lesssim m_Q/E$  for a quark of mass  $m_Q$  and energy  $E$  according to perturbative Quantum Chromodynamics (QCD) (“dead cone”). Another consequence is the suppression of energetic particles in the jet which has been observed already for  $c$ - and  $b$ -quark jets. The suppression of the forward particles can be explained by an application of the Modified Leading Logarithmic Approximation (MLLA) of perturbative QCD. In this paper we investigate whether this type of analysis can be carried out also for top-quark jets with the much higher heavy quark mass allowing for QCD tests in this new kinematic regime. The new aspect of this analysis is the finite lifetime of the top quark. We consider for simplicity the decay  $t \rightarrow b\ell\nu$ , where the  $b$ -quark radiates gluons as well and partially obscures the dead cone. Guided by the decay amplitude in leading order in  $\alpha_s$  for  $e^+e^- \rightarrow t\bar{t}$  we propose a method to separate the radiation by the  $\widehat{t\bar{b}}$  dipole in the decay process which is superimposed to the primary radiation from the  $\widehat{t\bar{t}}$  dipole involving the top-quark dead cone effect. The momentum distributions of partons or hadrons are determined for finite decay angles of the  $b$ -quark  $\Theta_b$  and extrapolated into forward direction  $\Theta_b = 0$  where the radiation from the decay process is expected to vanish. This method is successfully tested at the parton level and results obtained for hadrons are compatible with the MLLA relation within an accuracy of around 15%. Our calculations are carried out with the Pythia 8.3 Monte Carlo Event Generator.

## I. INTRODUCTION

Gluon emission from a coloured particle is an elementary process in QCD, it can be seen in analogy to photon emission from an electrically charged particle in QED. This radiation has a characteristic dependence on the mass of the primary particle which has been studied with its observable consequences in perturbative QCD [1, 2]. For an energetic heavy quark  $Q$  of mass  $m_Q$  and energy  $E_Q$ , such that  $E_Q/m_Q \gg 1$ , the probability for gluon emission at small emission angle  $\Theta_g$  and low energy  $\omega$ , can be written in leading perturbative order as

$$d\sigma_{Q \rightarrow Q+g} \simeq \frac{\alpha_s}{\pi} C_F \frac{\Theta^2 d\Theta^2}{(\Theta^2 + \Theta_0^2)^2} \frac{d\omega}{\omega}, \quad (1)$$

with angular cut-off  $\Theta_0 = m_Q/p_Q \simeq m_Q/E_Q$  at momentum  $p_Q$ ;  $\alpha_s$  denotes the strong coupling constant and  $C_F$  the QCD colour factor at the branching vertex  $Q \rightarrow Q + g$ . Therefore, for smaller emission angles  $\Theta \lesssim \Theta_0$ , gluon radiation is suppressed and vanishes in the forward direction. The depopulated region around the flight direction of the heavy quark is called “dead cone”. This depopulation increases with increasing mass. On the other hand, for large emission angles  $\Theta \gg \Theta_0$ , the gluon radiation pattern becomes identical to that of a light quark jet.

The dead cone effect has first been observed experimentally by the relative suppression of total particle multiplicity associated with heavy quark ( $c$ - and  $b$ - quark) production in  $e^+e^-$  annihilation already some time ago [3, 4]. Only recently the dead cone effect has been established by the ALICE collaboration [5]. The ALICE collaboration analysed charm-quark jets produced in  $pp$  collisions at the Large Hadron Collider and measured the angular dependence of the production of subjets with respect to the direction of the primary charm quark. They found a depletion in the forward direction as expected from QCD based Monte Carlo Event Generators (MCEG). Alternatively, the dead cone effect can be observed with momentum spectra of partons and hadrons which are expected to be suppressed at high momenta. This suppression has been investigated in an analytical approach within the Modified Leading Logarithmic Approximation (MLLA) [2]. Recently, this suppression of high momenta predicted for heavy quark jets has been observed in  $e^+e^-$ -annihilation at the LEP energy of 91.2 GeV and these results support the QCD expectations within MLLA; in particular, the dependence on the mass of the primary heavy quark has been confirmed by the comparison of charm-quark and bottom quark-jets [6].

In this paper we want to investigate how this type of analysis of the momentum spectra could be applied to the production of top quark jets. This would extend the dead cone study to the much higher mass of the top quark  $m_t = 172.52 \pm 0.33$  GeV [7–10] as a test of the underlying QCD theory but also of our understanding of the

hadronization effects in the presence of a large forward empty cone. A new feature in top production is the finite lifetime corresponding to the width  $\Gamma_t = 1.42_{-0.15}^{+0.19}$  GeV [7]. There are two aspects to be taken into account: first, in the decays  $t \rightarrow bW$  with  $W \rightarrow \ell\nu$ , which we consider for simplicity, there appears the coloured quark  $b$  from the decay in the final state which radiates itself and this radiation is superimposed over the top-quark Bremsstrahlung. Secondly, the finite lifetime will lead to a suppression of soft particles in the jet with energies of order  $\Gamma_t$  [11, 12].

It is therefore our primary aim to investigate the possibilities of how to separate the top-quark gluon radiation from the “background” of radiation from secondary decays. Two methods have been considered: one selects decay configurations of  $(t \rightarrow tb)$  with laterally emitted b-quarks, so that forward radiation ( $t \rightarrow tg$ ) can be separated. Secondly, from the measurement of the mass  $M(b\ell\nu)$  one can decide whether the emitted gluon comes from primary radiation with final top mass at  $M(b\ell\nu) \sim m_t$  or from the radiation from the b-quark in the top quark decay with  $M(b\ell\nu) < m_t$ . Such feasibility studies based on an angular analysis of subjet production have been performed by Maltoni et al. [13] with the result based on MCEG that a dead cone may be made visible in the high energy top-quark jet with the application of the two methods.

In this paper we investigate again the potential of the angular analysis, but our main aim is the study of feasibility to observe the dead cone effect from the suppression of the high momenta in the top quark fragmentation. Such a study is less dependent on the determination of the initial top quark direction as required in the angular analysis. This study is based mainly on Pythia 8.3 MCEG [14, 15]. The generator provides the initialization of the process according to the amplitude of a QCD matrix element and the generation of a parton cascade with a final transition to hadrons according to the Lund hadronization approach [16]. In addition we want to follow the main arguments also within the simplified treatment based on leading order perturbation theory, especially [12], and also on the results from the Modified leading logarithmic approximation [17] with the important concept of “angular ordering” [18, 19] built in which provides some analytical results on the jet evolution. In Section II, we discuss some of the theoretical tools and results used in this analysis. In section III we investigate the angular structure of top production events and study how well the top-quark radiation can be separated from the other processes, whereby we also address some aspects of hadronization. This study will motivate our procedure in the study of the momentum distributions and their separation from “background”. The momentum distributions obtained in this way will be compared to the MLLA expectations, thereby following and extending our previous analysis of c- and b-quark jet production [6] (Section IV). For this analysis, we apply the Pythia 8.3 MCEG [14] in its standard version. For hadrons we include charged and neutral particles as provided by the MC. The consequences of the finite width  $\Gamma_t$  of the top quark on the soft particle production are investigated based on a modified version of Pythia 8.3 in Section V. We consider here the reaction  $e^+e^- \rightarrow t\bar{t}$  at the c.m.s. energy  $\sqrt{s} = 1$  TeV which may become available in a future collider. Some aspects of the application to top quark jets in pp collisions are considered in Section VI.

## II. THEORETICAL CONSIDERATIONS

### A. Gluon emission from unstable top-quark in leading perturbative order

We begin with a description of some essential features of particle jet formation in the leading order of  $\alpha_s$ . In this approximation we consider the reaction  $e^+e^- \rightarrow t\bar{t}g$  where the main top-quark decay is  $t \rightarrow bW$  and we take into account here for simplicity only the leptonic decay channel  $t \rightarrow b\ell\nu$ . For this decay the gluon energy and the angular distribution have been calculated in the leading order of  $\alpha_s$  [11, 12] and the results can be written as [12]

$$\frac{1}{\sigma_0} \frac{d\sigma_g}{d\omega d\cos\theta_g d\phi_g} = \frac{\alpha_s C_F}{4\pi^2} \omega F, \quad (2)$$

$$F = |A|^2 + |B_1|^2 + |B_2|^2 - 2\text{Re}[B_1 B_2^*] + 2\text{Re}[A(B_1 - B_2)^*].$$

with

$$|A|^2 = -\frac{m_t^2}{(p_t \cdot k)^2} - \frac{m_t^2}{(p_{\bar{t}} \cdot k)^2} + \frac{2p_t \cdot p_{\bar{t}}}{p_t \cdot k p_{\bar{t}} \cdot k}$$

$$|B_1|^2 = -\frac{m_b^2}{(p_b \cdot k)^2} - \frac{m_t^2}{(p_t \cdot k)^2} + \frac{2p_b \cdot p_t}{p_b \cdot k p_t \cdot k}$$

$$|B_2|^2 = -\frac{m_b^2}{(p_{\bar{b}} \cdot k)^2} - \frac{m_t^2}{(p_{\bar{t}} \cdot k)^2} + \frac{2p_{\bar{b}} \cdot p_{\bar{t}}}{p_{\bar{b}} \cdot k p_{\bar{t}} \cdot k}$$

The amplitudes  $A, B_1$  and  $B_2$  are expressed in terms of the external particle momenta of the quarks  $p_i$  and the gluon  $k$  and correspond to the “dipoles” [17]  $\widehat{t\bar{t}}$ ,  $\widehat{t\bar{b}}$  and  $\widehat{\bar{t}\bar{b}}$ . The term with  $|A|^2$  corresponds to the emission of a

gluon from the top-quark as in Eq. (1), whereas the term  $|B_1|^2$  represents the decay of the top-quark  $t \rightarrow bW$  with associated gluon emission from the  $t$ - or  $b$ -quark, and accordingly the term  $|B_2|^2$  for the  $\bar{t}$  decay. The corresponding Feynman diagrams relevant for the top quark production and decay in the forward hemisphere are shown in Fig. 1.

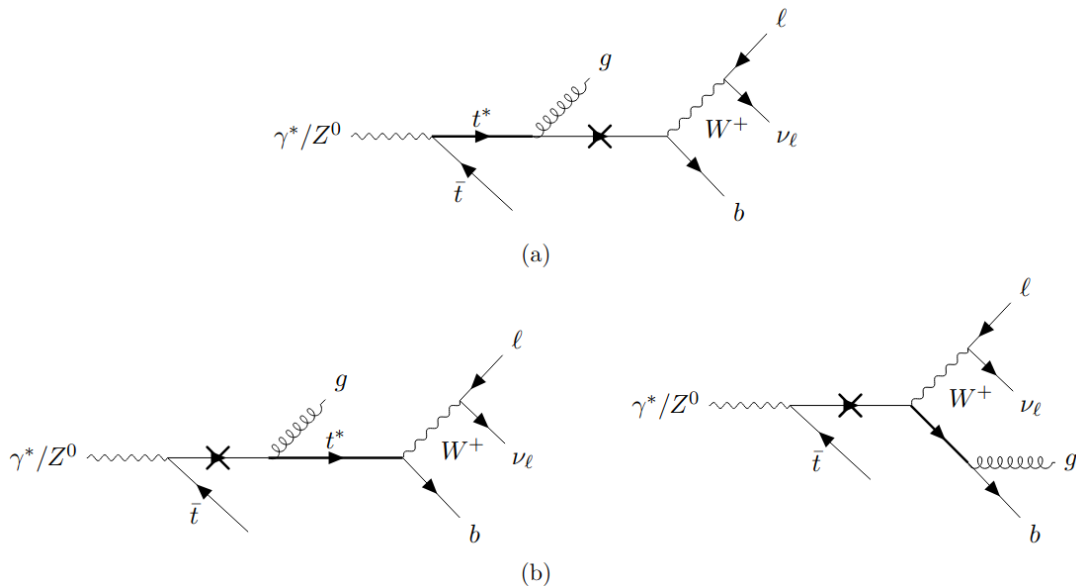


FIG. 1. Feynman diagrams for gluon emission in  $e^+e^- \rightarrow t\bar{t} \rightarrow bW^+ \bar{b}W^-$  relevant to the top quark hemisphere according to the decomposition Eq. (2). Heavy lines denote off-shell quarks. Panel (a) shows the correction to top production (amplitude  $A$ ), while panel (b) shows the corresponding corrections to top decay (amplitude  $B_1$ ), including gluon emission from the  $b$ -quark in the decay (according to [12]).

The two interference terms in Eq. (2) contain factors  $D_i$  depending on the top width  $\Gamma_t$ :

$$m_t^2 D_1 = \frac{m_t^2 \Gamma_t^2}{(p_t \cdot k)^2 + m_t^2 \Gamma_t^2} \quad (3)$$

for the  $t$ -quark and likewise for  $D_2$  with the  $\bar{t}$ -quark. As discussed in Ref. [12] it depends on the particular orientation of the gluon with respect to the  $t$ - and  $b$ -quarks whether the dependence of the cross section on the width  $\Gamma_t$  becomes observable. In PYTHIA 8.3 these width dependent terms are not included in the default version. They can be included within a special option and their effect is investigated in Sec. V with the result that for the application on momentum spectra of hadrons the effect is rather small of  $O(10\%)$ . So in the following sections III and IV we do not consider these effects.

In the following we study the results for the hemisphere of the top quark only which is also relevant for the application to  $pp$ -collisions. The above results in Eq. (2) can be written for the top quark hemisphere in the approximation for massless gluons with small gluon angle  $\Theta_g$  to the top-quark and  $\Theta'_g$  to the  $b$ -quark at high primary energies  $E_t$  as

$$\omega^2 |A|^2 = \frac{4\Theta_g^2}{(\Theta_g^2 + \Theta_0^2)^2} + O(\Theta_0^2) \quad (4)$$

$$\omega^2 |B_1|^2 = \frac{8(1 - \beta\beta' \cos \gamma)}{(\Theta_g^2 + \Theta_0^2)(\Theta_g'^2 + \Theta_0'^2)} - \frac{4\Theta_0^2}{(\Theta_g^2 + \Theta_0^2)^2} - \frac{4\Theta_0'^2}{(\Theta_g'^2 + \Theta_0'^2)^2} + O(\Theta_0^4, \Theta_0'^4) \quad (5)$$

where  $\beta, \beta'$  denote the  $t$ - and  $b$ -quark velocities  $\beta = p_t/E_t$ ,  $\beta \approx 1 - \frac{1}{2}Q_0^2$  and  $\beta' = p_b/E_b$ ,  $\beta' \approx 1 - \frac{1}{2}Q_0'^2$  with  $\Theta_0' = m_b/p_b$  and  $\gamma$  denotes the decay angle of the  $b$ -quark with respect to the  $t$ -quark direction in the  $e^+e^-$  c.m.s.

In the leading order calculation considered here, we note that the  $b$ -quark radiation comes from the  $t\bar{b}$  dipole. Thus  $b$ -quark radiation is associated with additional radiation from the top quark, and even if the  $b$ -quark decays with large angle  $\gamma$  laterally such that the  $b$ -quark fragments are well separated from the top quark fragments, there remains some radiation in the top quark direction ( $\propto 1/(\Theta_g^2 + \Theta_0^2)$ ), finite at  $\Theta_g = 0$ , represented by the first term in Eq. (5), while the two other terms vanish at high energies. However, we observe that the leading term in  $|B_1|^2$  vanishes at high energies for decays of the  $b$ -quark in the forward direction  $\gamma = 0$ . This holds also for the gluon momentum spectrum after integration over the gluon decay angles  $\Theta_g, \Theta'_g$ .

In order to obtain the momentum spectra of partons from top-quark fragmentation we have to integrate these distributions over the gluon emission angles and obtain contributions from the different components. For  $|A|^2$  we get at large angles  $\Theta_g$  the integral over  $d\Theta_g^2/\Theta_g^2$  which yields a contribution logarithmically rising with the upper limit. For the terms in  $|B_1|^2$  the integrals over  $\Theta_g, \Theta'_g$  are dominated by the small angle emissions near  $\Theta_0, \Theta'_0$  and we can approximately write for the angular integral

$$\omega^2 \langle |B_1|^2 \rangle \simeq 8c_1(\gamma)(1 - \beta\beta' \cos \gamma) + 4c_2\Theta_0^2 + 4c_3\Theta_0'^2 \quad (6)$$

At the high energies considered here the second and third terms are negligible and so  $\langle |B_1|^2 \rangle$  decreases with decreasing decay angle  $\gamma$  for  $t \rightarrow b$ . For our scenario with  $E_t = 500$  GeV we have  $\beta = 0.94$  and  $\beta' = 0.995\dots 0.9999$  for the b-quark momenta in the region 20 - 450 GeV. While in the first term  $c_1(\gamma)$  remains finite, there is also the factor  $(1 - 0.94 \cos \gamma)$  which nearly vanishes for the emission of the b-quark parallel to the top quark. This behaviour is well understood and, in fact, for particles of equal mass and velocity the factor in Eq. (6) would reduce to

$$\omega^2 \langle |B_1|^2 \rangle \simeq (1 - \cos \gamma) + O(\Theta_0^2), \quad (7)$$

which vanishes for  $\gamma \rightarrow 0$ , as by a Lorentz boost into the rest frame the two particles at rest would clearly not radiate. On the other hand, the  $|A|^2$  term remains large in the limit  $\gamma \rightarrow 0$  in comparison to the  $|B_1|^2$  term. We conclude that for the b-quark emitted in the top-quark decay in the forward direction the radiation from the  $\widehat{t\bar{b}}$  dipole nearly vanishes. This property opens the possibility to obtain separately the gluon radiation pattern of the stable top-quark represented by the  $|A|^2$  term in Eq. (2).

As the two jets produced by the top and the b-quark cannot be separated directly if they are parallel, we consider the possibility to determine the momentum spectra of the gluons at larger relative angles  $\gamma$  and extrapolate the results so obtained to the angle  $\gamma = 0$ . The same should also apply for the final momentum spectra of partons or hadrons as they are generated by the further evolution of the primary gluon. If the  $\widehat{t\bar{b}}$  dipole does not radiate gluons, neither partons nor hadrons will evolve from this source. In this way the momentum spectrum corresponding to a stable top quark can be obtained by extrapolation.

We note that in the leading approximations Eqs. (2), (5) the momentum spectrum factorizes from the angular distributions and the momentum spectrum changes with angle  $\gamma$  only in magnitude not in shape, but this does not hold in general. For parton and hadron spectra, besides the  $\gamma$  dependence in Eq. (6) there is also a change of the dipole radiation with this angle  $\gamma$  as a consequence of the jet evolution. The extrapolation function for the parton and hadron momentum spectra will be determined here from the MCEG.

## B. Multiple gluon emission and angular ordering

In this subsection we will recall a few properties of jet evolution which are of particular relevance for our subsequent analysis. The primary gluon emitted from the initial quark is the source for the subsequent parton production which can be described by an evolution equation for the bulk of particles within the Leading and Modified Leading Logarithmic Approximation (DLA and MLLA) in a one loop order approach. For illustration we recall the evolution equation in DLA for the distribution  $D_q^p$  of partons  $p$  with energy  $\omega$  in a jet of opening angle  $\Theta$  for a primary quark  $q$  of energy  $E_q$  [17]

$$D_q^p(\xi, y_\Theta) = \delta_q^p \delta(\xi) + \int_0^\xi d\xi' \int_0^{y_\Theta} dy' (C_F/N_c) \gamma_0^2(y') D_g^p(\xi', y') \quad (8)$$

with  $\xi = \ln(E_q/\omega)$ ,  $y_\Theta = \ln(\omega\Theta/Q_0)$ ,  $\gamma_0^2 = 4N_c/(b \ln y')$ ,  $b = \frac{11}{3}N_c - \frac{2}{3}n_f$  and cut off parameter  $Q_0$ . Because of ‘‘angular ordering’’ [18, 19] the secondary particles are emitted within the cone given by the production angle of the primary gluon with parameters  $\xi', y'$ , the production of particles outside this cone vanishes in the azimuthal average<sup>1</sup>. For a primary heavy quark the modified angular distribution as in Eq. (1) has to be inserted under the integral above for the first emission.

As an illustration of this production process with angular ordering we show in the upper panels of Fig. 2 the distribution of the final partons over the rescaled angular variables  $(X, Y)$  for a few typical events obtained by the Pythia 8.3 MCEG of the process  $e^+e^- \rightarrow t\bar{t}$  at 1 TeV for stable top-quarks with

$$X = (\Theta/\Theta_0) \cos \phi, \quad Y = (\Theta/\Theta_0) \sin \phi. \quad (9)$$

<sup>1</sup> For an introductory outline of intra-jet coherence phenomena, see for example Refs. [17, 20].

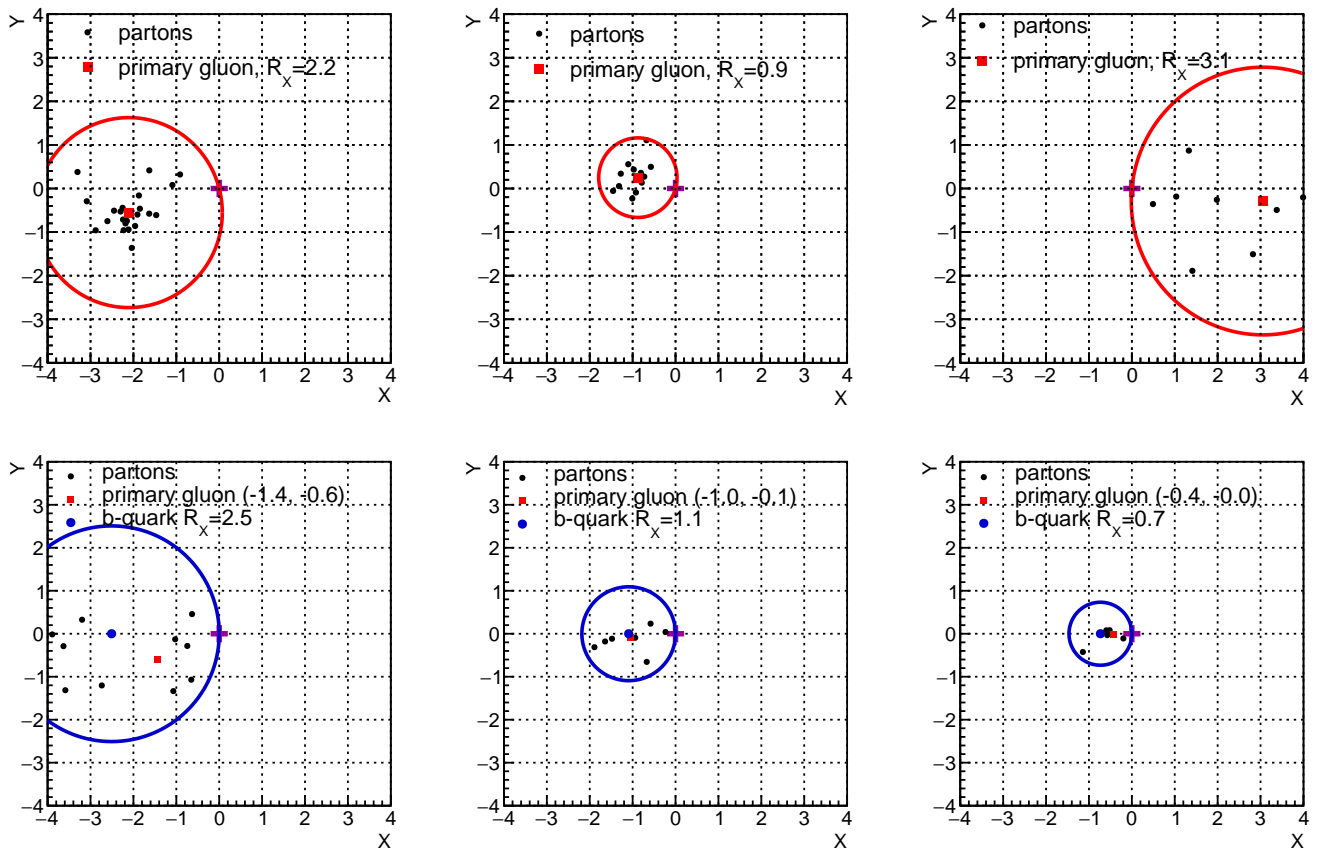


FIG. 2. Scatter plots for three representative events from  $e^+e^- \rightarrow t\bar{t} + X$  with stable top-quark at  $\sqrt{s} = 1$  TeV (upper panels), showing the distribution of partons from top-quark fragmentation over the angles  $X$  and  $Y$  in Eq. (9) in units of the dead cone angle  $\Theta_0$  with the top-quark direction in the centre  $(0,0)$  (shown as cross): the primary gluon as red point at angle  $R_X = \Theta/\Theta_0$  to the centre surrounded by the emitted partons (black points) limited by the same angle  $R_X$  (red circle) as required by “angular ordering”; lower panels: Scatter plots as above but for events with top quark decay  $t \rightarrow b\ell\nu + g$  for primary gluons triggered with  $X_g < 0$  shown as red square and the b-quark as blue dot rotated into negative  $X$ -direction ( $Y = 0$ ) and with  $X_b < -0.5$ . The emitted partons come mainly from the b-quark and are found inside the blue circle around the b-quark position as required by angular ordering (lower panels); here  $\Theta_0 = 20^\circ$  at 1 TeV (from Pythia 8.3).

Here the production angle  $\Theta$  of a parton is measured with respect to the top quark direction in the center at  $(0,0)$  and is normalized to the dead cone angle  $\Theta_0 = m_t/E_t$ , and  $\phi$  is the azimuth around the top direction with  $\phi = 0$  for the initial  $e^-$  as defined in the App. C. The production angle of a primary gluon is indicated by the red point, then the partons emitted from this gluon, because of angular ordering, fall inside the circle around the gluon whose radius is defined by the distance to the top-quark direction at  $(0,0)$  (the red circle through the origin). Within the viewpoint of Eq. (8) an estimate of energy and angle of the primary gluon is obtained from the sum over the 4-momenta of the final partons except for the initial quark itself<sup>2</sup>.

In the realistic case of an unstable top quark we have in addition to the term  $|A|^2$  for the  $t\bar{t}$  antenna in Eq. (2) also terms  $|B_{1,2}|^2$  with the gluon emission from the  $b$ - and  $\bar{b}$ -quarks. In this leading order approximation in  $\alpha_s$  the primary gluon is radiated from either one of the superimposed dipoles and therefore it will be produced either from the top- or from the b-quark. As a consequence, individual events should show dominantly radiation from either source, t- or b-quark. This view is confirmed by the observation from the MCEG that, with a trigger on a particle in the top quark jet, the emission from the b-quark jet was much reduced from the average. In this approximation the primary gluon can be reconstructed again as the sum over all final partons in the event.

This situation can be visualized again in the  $(X, Y)$  angular scatterplot of final partons. We orient the event in such a way that the b-quark moves in the direction of the negative  $X$ -axis. Then, if we select a particle with  $X_g > 0$

<sup>2</sup> see also [13], where the primary gluon is estimated from the NLO matrix element by combining the final gluons (up to two).

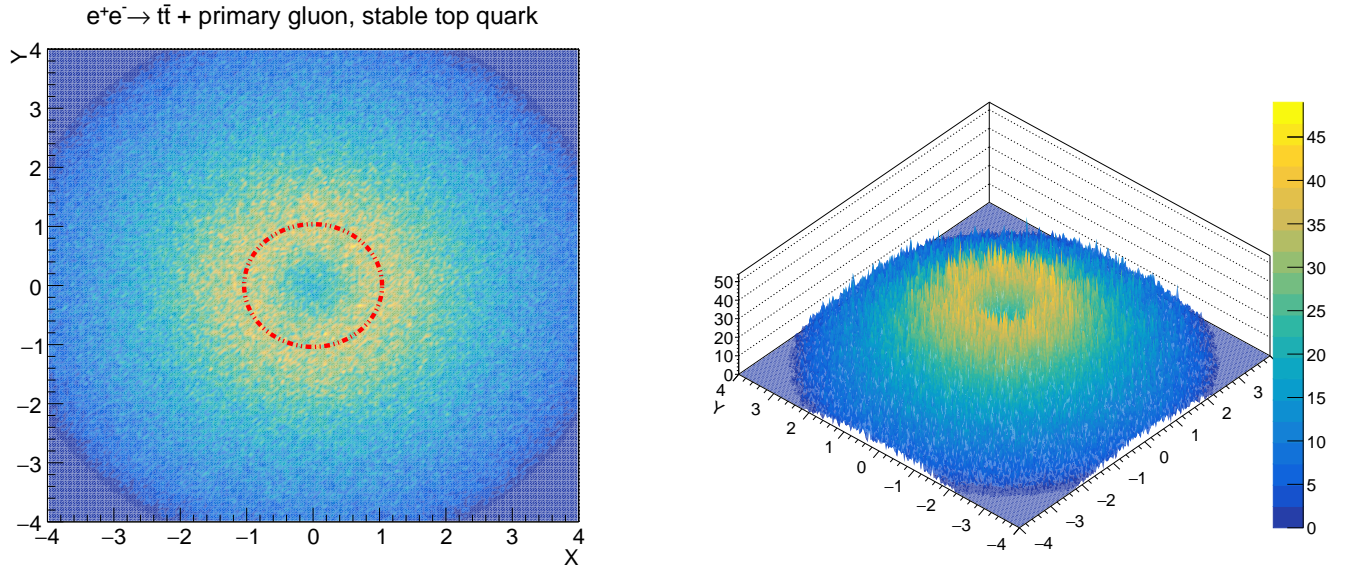


FIG. 3. Angular distribution of the reconstructed primary gluon in  $e^+e^- \rightarrow t\bar{t} + \text{partons}$  at 1 TeV around the top-quark direction for stable top quarks: the left panel shows the distribution in the rescaled angles  $(X, Y)$ , defined in Equ. (9), with the dead cone boundary  $R_X^2 = X^2 + Y^2 \simeq 1$  and the suppression in the centre, the right panel shows the corresponding gluon density. At this energy the dead cone angle  $\Theta_0 \simeq 20^\circ$  and the forward hemisphere ends at  $R_X \simeq 4.5$ . Data generated with Pythia 8.3.

it will primarily come from the gluon emitted from the top-quark and the parton distribution will look similar to the events in the upper channels.

In the lower panels of Fig. 2 we show representative events with primary gluons found in the left hemisphere with  $X_g < 0$ . They can be related to the emission from b-quarks centered along the negative  $X_b$  axis with  $X_b < -0.5$ . The partons are found within a circle around the b-quark limited by the direction of the top quark at  $(0,0)$  as required by angular ordering in the radiation from the  $t \rightarrow b$  transition. While in these events all partons are confined into the blue circle there are also events with partons outside which have its origin from t- and b-quark radiation processes.

These figures show the important role played by the angular ordering condition: without this restriction b-quarks at small angles  $X_b$  would emit a large fraction of partons into the right hemisphere. With this condition fulfilled, it is of advantage to determine the top quark fragmentation products only from particles in the right hemisphere  $X > 0$  where the b-quark radiation is suppressed.

### III. ANGULAR STRUCTURE OF TOP-QUARK JET

In this section, we investigate various aspects of the angular distributions in the top-quark jet, especially on the role of the additional decay  $t \rightarrow bW$ , under the assumption that the top-quark direction is known, as it is in the MCEG. In the experiment the determination of the top-quark direction is limited not only by fluctuations of final-state hadrons in the jet, but also by the uncertainty in the reconstructed neutrino direction [21, 22]. For the di-lepton final state a resolution for the neutrino 4-vector of less than 5% for 80% of the events is predicted [21]. Therefore, the results reported here can be compared to the experiment only after corresponding averaging. However, they are also important in the design of our subsequent study of momentum distributions.

#### A. Stable top-quark

We begin with an analysis for the case of a hypothetical stable top quark which can be treated with the methods discussed before [6]. These results serve as a benchmark in the study of unstable top quarks to test the validity of the background subtraction from the decay processes. We consider the primary reaction  $e^+e^- \rightarrow t\bar{t}$  at the c.m.s. energy  $\sqrt{s} = 1$  TeV and generate events using the Pythia 8.3 MCEG. In the soft and collinear approximation to the radiation process the emission of a gluon by the stable top quark is given in leading perturbative order by Eq. (1) with angular

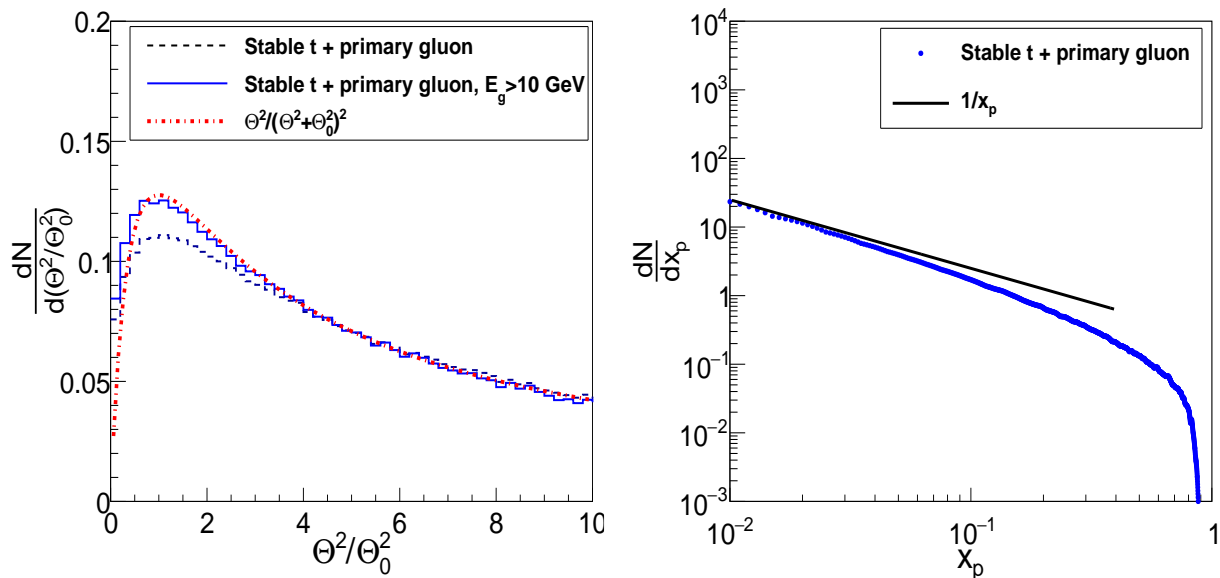


FIG. 4. Distribution of the reconstructed primary gluon as in Fig. 3 in the rescaled opening angle  $\Theta/\Theta_0$  for stable top-quark production without and with gluon energy cut-off  $E_g > 10$  GeV and distribution in momentum fraction  $x_p$ , both in comparison with the approximate analytic form Eq. (1).

cut-off  $\Theta_0 \simeq m_t/E_t$ , with  $E_t = 500$  GeV the dead cone angle is  $\Theta_0 \sim 20^\circ$ . This angular distribution of the gluon reaches its maximum at  $\Theta = \Theta_0$  and is suppressed at smaller angles inside the dead cone region.

From the parton cascade generated by the primary  $t\bar{t}$  state, we reconstruct the primary gluon corresponding to the leading order process  $t \rightarrow tg$  approximately from the sum of all partons in the top-quark hemisphere besides the top quark itself, i.e. the final top-quark represents a jet by itself as discussed in the last section. This approximation is also suggested by the large energy fraction  $\langle x_t \rangle = 0.92$ , see Eq. (14) below, which the leading heavy quark takes in the fragmentation. In Fig. 3 we show the 2-dimensional angular distribution of these primary gluons for the process  $e^+e^- \rightarrow t\bar{t}g$  at 1 TeV in the rescaled angular variables  $(X, Y)$  from Eq. (9) in the top-quark hemisphere. The distribution clearly shows the suppression in the center  $(X, Y) = (0, 0)$  corresponding to the top-quark flight direction.

In Fig. 4, left panel, we show the distribution of the reconstructed primary gluon in the polar angle  $\Theta$ . The approximate formula Eq. (1) describes the forward suppression and the overall shape quite well but with some deviations at small angles. A better description is obtained after a cut on the gluon energy  $E_g > 10$  GeV. Also the distribution of the fractional momentum  $x_p = p_g/E_t$  shown in the right panel follows the distribution  $dN/dx_p \propto 1/x_p$  as in Eq. (1) in the region of small energy. So the primary gluon constructed in this approximate way follows the expectations of the leading  $\alpha_s$  order prediction in Eq. (1) where some small deviations are caused by low energy particles close to the edge of the forward hemisphere. As the effect is small with respect to our subsequent analysis we do not take it in a special account in the following.

The corresponding distributions for secondary partons are shown in Fig. 16 in the App. A. The central dead cone is partially filled but still visible.

## B. Decaying top-quark, 2-dim angular distributions

Now we turn to the realistic case of unstable top-quark with decay width  $\Gamma_t = 1.42$  GeV. The main decay channel is  $t \rightarrow bW$ , where we consider only processes with the leptonic decays  $W \rightarrow e\nu$ . In that case an additional source of gluon radiation is generated by the b-quark as discussed in the previous section.

In this decay process it is necessary to identify the b-quark jet and the gluon jet separately and the determination of a single gluon from the sum over all particles is not sufficient. In order to combine partons or hadrons into separate jets, we apply the jet reconstruction program Fastjet [23, 24] with parameters  $R = 0.2$  for the angular radius and  $p = 1$  corresponding to the  $k_T$ -algorithm. This radius is comparable to values used in other heavy-flavour and b-quark analyses [25–27]. A larger radius like  $R = 0.4$  would not separate the b-jet and the gluon jet in a substantial fraction

of events. In leading perturbative order as in Eq. (2) we expect a b-jet and one additional gluon jet which is either emitted from the top-quark or from the b-quark. Out of the jets found by the program we identify the b-quark jet as the one which contains the b-quark or the B-hadron. If more than two jets are obtained, we combine all jets besides the b-quark into one final gluon jet.

The appearance of the two processes with amplitudes  $A$  and  $B_1$  in Eq. (2) from top quarks with different virtual masses is visualised in Fig. 5. In the left panel a plot of the invariant masses  $M(b\nu + g)$  versus  $M(b\nu)$  is shown for the parton final state, in the right panel for hadrons with b-quark replaced by B-hadron. The presence of two stripes is clearly visible in both figures, the events fall with a large probability into one of the two classes. The vertical stripe of events corresponds to a fixed mass  $M(b\nu)$  or  $M(B\nu)$  near the top mass and represents the events with gluon emission from the primarily produced virtual top-quark  $t^* \rightarrow tg$  as in the case of stable top-quark ( $t\bar{t}$  dipole). The horizontal band corresponds to events from the  $t\bar{b}$  dipole with the invariant mass of the particles  $M(b\nu + g)$  or  $M(B\nu + g)$  near the top-quark mass corresponding to the decay  $t \rightarrow b\nu + g$  with variable virtual b-quark or t-quark mass. The maximal density along the stripes is obtained at the mass scale  $m_t = 172.5$  GeV for the respective mass combinations, where the gluon has minimum momentum; in this mass range both components overlap. It is remarkable that the stripes for hadrons and partons show a rather similar density over the stripes although hadrons are generated in a later phase of the jet evolution with a higher particle multiplicity.

There are events in Fig. 5 which cannot be directly attributed to one of the two stripes. These could be events from processes with more than one gluon, such as expected in non-leading order for events with two gluons, one from t- and one from b-quark. There could also be events where in a top quark decay one particle is lost by leaving the hemisphere of the produced primary top-quark considered here, which would move the event outside the stripe. Such effects could contribute to a systematic error which we will estimate for our final results.

At first, we look again at the 2-dimensional  $(X, Y)$  angular distribution of the gluon jets as in the case of the stable top-quark. The additional radiation from the b-quark can be made better visible by selecting events with the

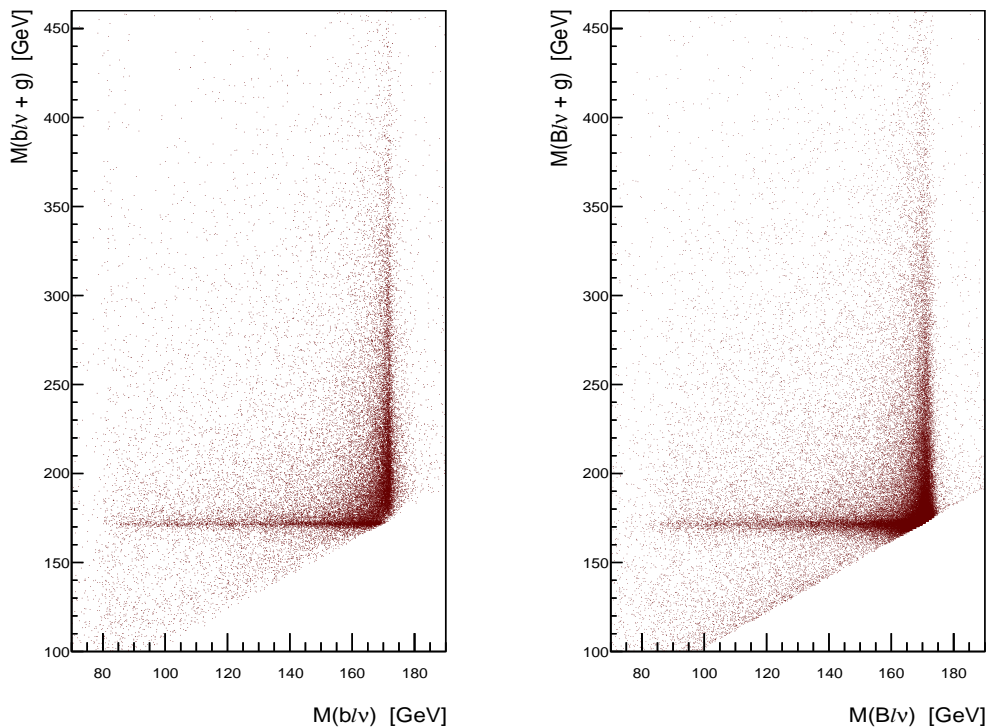


FIG. 5. The invariant masses  $M(b\nu + g)$  vs.  $M(b\nu)$  in  $e^+e^- \rightarrow t\bar{t} + X$  with  $b$  and  $g$  representing jets reconstructed from the final partons (left panel) and  $M(B\nu + g)$  vs.  $M(B\nu)$  from the final charged and neutral hadrons (right panel). The narrow stripes form near the top mass  $m_t = 172.5$  GeV. The vertical stripe corresponds to the processes of hard gluon radiation from the top-quark  $t^* \rightarrow tg$ , the horizontal stripe to the top-quark decay with gluon emission  $t \rightarrow b\nu + g$ .

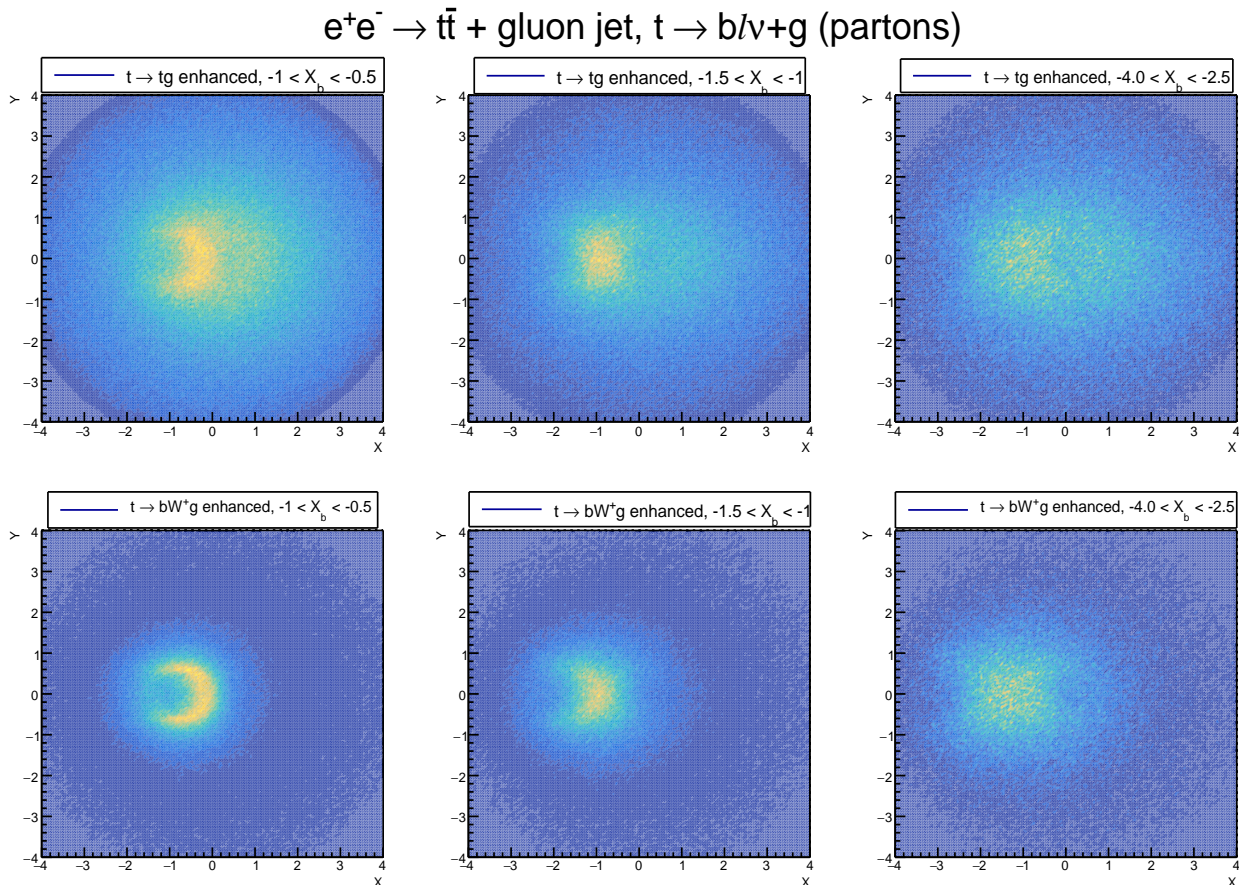


FIG. 6. Distribution of gluon jets constructed from partons over the angles  $(X, Y)$  of Eq. (9) around the top-quark at  $(0,0)$  with the b-jet pointing into the negative X-axis, for processes dominated by gluon emission  $t \rightarrow tg$  (upper row) and dominated by top decay  $t \rightarrow b\bar{\nu} + g$  (lower row) according to selection of vertical or horizontal stripes in Fig. 5 respectively for masses 170-175 GeV; for different angles of the b-quark to the top quark  $X_b$ , increasing from left to right, b-jets removed. The upper row reflects at low intensity the gluon radiation from the top-quark around a circle of radius  $R_X = 1$  in  $X, Y$  units around the top direction with the dead cone in the center, nearby on the left a yellow hot spot limited by two circles, on the left by the empty cone of the b-jet of angular radius  $R = 0.2$ , or  $R_X = 0.6$ , and on the right by the circle through the origin required by angular ordering. The lower row shows the gluon radiation of the b-quark from top decay outside the angular radius  $R = 0.2$ ; the wider gluon radiation from the top quark as seen in the upper figures with  $R_X \sim 1$  is suppressed.

b-quarks emitted away from the top direction. For a better presentation we rotate the event around the top quark direction so that the b-quark points into the negative X-axis. Results for the gluon jets are shown in Fig. 6 for three different intervals of the b-quark angles  $X_b$  in between -4.0 and -0.5, the b-quark jets are removed from the figure. The upper row shows the events selected from the vertical stripe for masses  $m(b\bar{\nu}) = 170-175$  GeV, i.e. enhanced  $t \rightarrow tg$  processes, the lower row selected from the horizontal stripe with enhanced  $t \rightarrow b\bar{\nu} + g$  processes within the same top-quark mass interval and with  $m(b\bar{\nu}) < 160$  GeV.

In the upper part of Fig. 6 the radiation from the top quark around the center  $(0,0)$  with a ring of radius  $R_X \sim 1$  with  $R_X = R/\Theta_0$  in  $(X, Y)$  units, i.e. at the dead cone angle  $\Theta = \Theta_0$ , is apparent at all b-quark angles  $X_b$  and also the dead cone in the center is visible as depletion of central density, but less pronounced as in Fig. 3. The narrow yellow stripe left from the center represents the gluon radiation from the b-quark outside the angular radius  $R = 0.2$  of the b-quark jet corresponding to  $R_X \approx 0.6$ , while the interior is removed from the figure. This additional radiation from the b-quark is limited on the right side by the circle centered at the b-quark decay angle  $X_b$  and going through the top-quark direction at  $(0,0)$  because of the angular ordering condition (see Sec. II B and Fig. 2, bottom panels). This b-quark radiation decreases with increasing angle  $X_b$  because of the related decreasing b-quark energy. We conclude, that our selection of events from the vertical stripe in Fig. 5 does not exclude the events with gluons from b-quark altogether. The presence of b-quark jets signals the presence of the  $t\bar{b}$  dipole with amplitude  $B_1$  in Eq. (2), which also contributes to a partial filling of the dead cone as will be discussed further below.

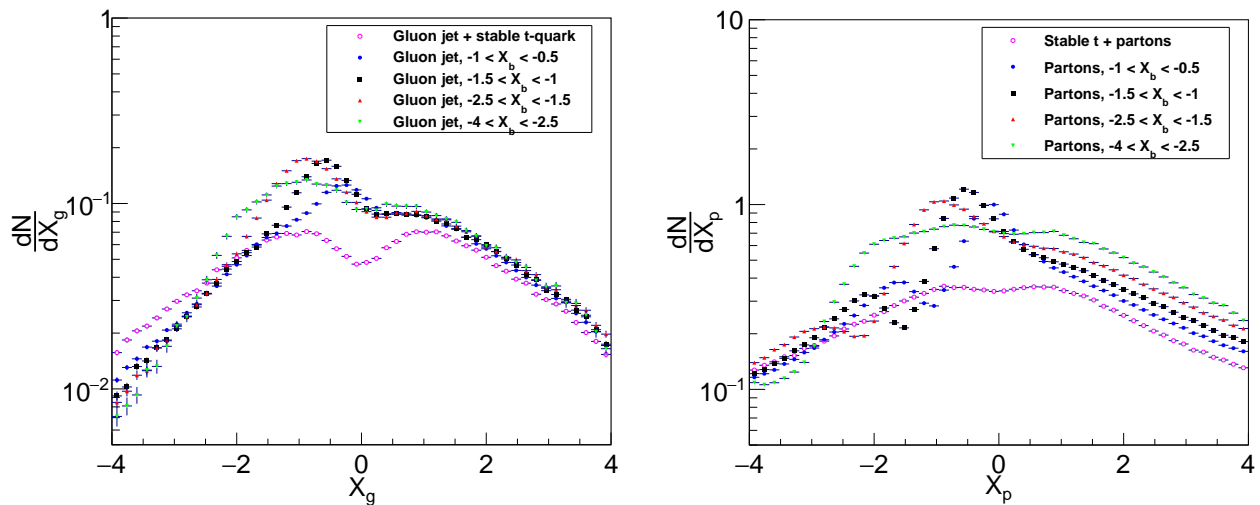


FIG. 7. Distribution over angle  $X_g$  of gluon jets, from events dominated by emission  $t \rightarrow tg$ , along central stripe through  $(X, Y)$  scatter plot in Fig. 6, upper row, within  $-\frac{1}{2} < Y < +\frac{1}{2}$  for different regions in the b-quark jet scattering angle  $X_b$ . The radiation from the  $\hat{t}\hat{b}$  dipole is superimposed to the radiation from the stable top-quark and is strongest in top quark direction at  $X_g = 0$  (left panel); the corresponding distribution for partons in the same central stripe show a stronger separation of distributions for  $X_g \gtrsim 0$  with angle  $X_b$  (right panel).

The panels in the lower part of Fig. 6 show the angular distribution of gluon jets for events along the horizontal stripe in Fig. 5 with gluons from top quark decays enhanced. Indeed, the dominant feature is now the radiation of half-moon like shape around the b-quark jet outside the angular radius  $R = 0.2$  and inside the circle through the origin  $(0, 0)$  required by angular ordering, with little or no evidence for the top quark radiation around the center with radius  $R_X \sim 1$ .

At much lower intensity there appears a halo of radiation around the b-quark direction of larger radius  $R_X \approx 2$ . This radiation could come from events where a gluon emitted from the b-quark is combined with partons from the top-quark and therefore escapes the angular ordering condition. Such events appear as we have restricted ourselves to single gluon emission processes as in the leading perturbative order.

In a corresponding procedure we also studied the 2-dimensional  $(X, Y)$  distributions for final state hadrons. Two jets are constructed and the one with a B-hadron is chosen as b-quark jet, the other one as gluon jet. The distributions for gluons from the  $t \rightarrow tg$  emission process indicates again a dead cone surrounded with a circular distribution of radius  $R_X \sim 1$ , more details are presented in the App. A, Figs. 17 and 18.

### C. Decaying top-quark, angular distributions within stripe along X direction

In order to study the central region around the dead cone in greater detail we consider in Fig. 7 the distribution of gluon jets and partons along the  $X$  axis in a horizontal stripe of width  $-\frac{1}{2} < Y < +\frac{1}{2}$  of the Fig. 6, upper row. The dip of the distribution visible for the stable top-quark at the center is largely filled for the unstable top-quark. The maximum reflects the edge of the jet where gluons emitted from the b-jet are outside the jet cone of radius  $R=0.2$ . These gluons from b-decay are restricted to  $X_g < 0$  because of angular ordering (see Sec. II). There is some flow beyond this limit especially for the smallest angles  $X_g$  which could come from a mismatch of partons generated by the MC and partons combined into a jet. While for large b-quark angles  $X_b < -2.5$  (green data points) the dead cone is indicated as dip around  $X_g = 0$ , the evidence is reduced for smaller angles  $X_b$ . At the smallest angle  $X_b < -0.5$  there is some excess of parton flow into the right hemisphere  $X > 0$ .

The behavior of these distributions can be qualitatively described in terms of the superposition of the two dipoles  $\hat{t}\hat{t}$  and  $\hat{t}\hat{b}$  represented by the amplitudes  $A$  and  $B_1$  in Eq. (2). The contribution of the b-quark amplitude is not directly known, as we have reduced its contribution by our vertical mass cut, so we calculate this contribution with the full density  $|B_1|^2$  for reference. The distributions  $dN/dX_g$  along the horizontal stripe can be calculated with  $\Theta_g = X_g\Theta_0$  and  $Y = 0$ . Furthermore, we have to express the variables  $\Theta', \phi'$  referring to the b-quark direction by  $\Theta, \phi$  in reference

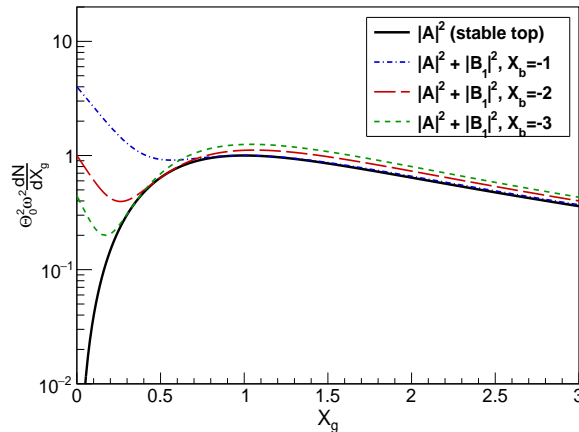


FIG. 8. Distribution of gluon jets along the  $X$ -axis of the  $(X,Y)$  scatterplot according to Eq. (11) for different b-quark angles  $X_b$  with contributions from amplitude  $A$  as for stable top-quark with dead cone and from  $B$  representing the  $\hat{t}\hat{b}$  dipole.

to the t-quark. Because of the strong collimation of the radiation from the b-quark, we approximate

$$\Theta'_g \approx \Theta_g - \Theta_b \quad (10)$$

for the region  $X_g > 0$  that is away from the b-quark position and this approximation should improve with increasing  $X_g$ . For small angles and high energies with  $\beta \approx 1 - \frac{1}{2}\Theta_0^2$ ,  $\beta' \approx 1$ ,  $\Theta'_0 \approx 0$  and noting that  $dXdY = d\cos\Theta d\phi \approx \Theta d\Theta d\phi$  we obtain the result for  $dN/dX_g \propto F$  in the top-quark hemisphere using Eqs. (4) and (5)

$$\begin{aligned} \frac{dN}{dX_g} &\propto |A|^2 + |B_1|^2 \quad (11) \\ \Theta_0^2 \omega^2 |A|^2 &= \frac{4X_g^2}{(X_g^2 + 1)^2}, \\ \Theta_0^2 \omega^2 |B_1|^2 &= \frac{4(1 + X_g X_b)^2}{(X_g^2 + 1)^2 (X_g - X_b)^2}. \end{aligned}$$

and this distribution is presented in Fig. 8 in the region  $X_g > 0$ .

The figure shows that the dead cone, i.e. the dip at the center  $X_g = 0$  of the  $A$  amplitude (stable t-quark) is filled by the contribution from the  $\hat{t}\hat{b}$  dipole (amplitude  $B_1 \propto 1/X_b^2$  decreasing with increasing  $X_b$ ). On the other hand, at larger angles  $X_g$  the contributions from the large b-quark angles  $X_b$  dominate. This increase is illustrated by the respective values of  $dN/dX_g$  for the gluon angles  $X_g = 1$  and  $2$  in Tab. I. The data in Fig. 7 show indeed, that at the center  $X_g = 0$  the lowest density appears for the largest angle  $X_b$  (green curve). With increasing b-quark angles  $X_b$  the curves cross and the density  $dN/dX_g$  for the largest b-quark angle  $X_b$  dominates. The effect is more evident for the parton final state in the right panel of Fig. 7 with a much larger separation of the data for different angles  $X_b$ . The same type of analysis has also been performed for the final state hadrons and the results are shown in Fig. 19 of App. A. The results are similar and again the hadrons for large b-quark angles  $X_b$  have a higher density as those for small angles, contrary to naive expectation from b-quark bremsstrahlung.

$X_g$	$\frac{dN}{dX_g}(X_g) _{\text{stable top}}$	$-1 < X_b < -0.5$	$-1.5 < X_b < -1$	$-2.5 < X_b < -1.5$	$-4 < X_b < -2.5$
1.0	0.072	0.081	0.082	0.087	0.098
2.0	0.051	0.056	0.057	0.058	0.059

TABLE I. Values of  $\frac{dN}{dX_g}$  at  $X_g = 1$  and  $X_g = 2$  for the stable-top projection and for gluon jets in five  $X_b$  intervals.

This characteristic ordering of spectra, especially for partons and hadrons, shows that the central dead cone region is not simply filled by the b-quark radiation but the  $\hat{t}\hat{b}$  dipole also radiates from the top quark. The intensity of radiation into the right hemisphere opposite to the b-quark direction even increases if the b-quark decay angle  $X_b$

is increased, contrary to the expectation from b-quark bremsstrahlung. However, for gluon jets both for parton and hadron final states this increase is smaller in the data than expected from the calculations in Fig. 8, this follows from the selection of events with emission  $t \rightarrow tg$  preferred. The influence of the b-quark to the right hemisphere with  $X > 0$  by bremsstrahlung is limited by angular ordering and its influence here is seen only in a very small angular region near the center out of the full forward hemisphere of the top production. We therefore construct the momentum distribution of partons and hadrons from top-quark decay from their distribution in the right hemisphere  $X_p > 0$  multiplied by factor 2.

#### D. Summary on angular distributions

We summarize these studies on the angular structure of the top-quark jet in the  $(X, Y)$  scatter plots by the following observations. A broad distribution of particles extends over a ring of radius  $R_X \sim 1$  in the rescaled angles  $\Theta/\Theta_0$ . A depletion from the dead cone in the center along the top quark direction is visible for the primary gluon jets constructed from partons or hadrons. This is achieved after selecting events with lateral b-quark emission and the decay products with masses  $M(b\nu)$  or  $M(B\nu)$  near the top-quark mass  $m_t$ . This selection on masses reduces the contributions from the  $\widehat{tb}$  dipole with radiation from b- and t-quark but does not eliminate them. A clear evidence for the radiation from this dipole follows from the dependence of the parton and hadron spectra at  $X > 0$  on the b-quark angle  $X_b$ . The radiation from the b-quark is limited to the left hemisphere  $X_g < 0$  because of angular ordering. At the level of final state partons or hadrons the separation of events with distinguishable top fragmentation is still possible while the dead cone depletion in the center is less clearly visible. From Figs. 6, 17 and 18, we consider the contribution of the b-quark jet into the hemisphere with  $X > 0$  limited to a small angular region around the center near  $\Theta = 0$  and we will next construct the inclusive parton and hadron distributions from top-quark fragmentation for the hemisphere of the top-quark  $0 < \Theta < \pi/2$  from the particles in the right hemisphere with  $X_{p,h} > 0$  in Fig. 18.

### IV. DISTRIBUTION OF PARTICLE MOMENTA IN TOP-QUARK JETS AND MLLA PREDICTIONS

#### A. Reconstruction of parton and hadron momentum distributions

The study of the angular distribution of particles around the top quark direction provides evidence for the dead cone effect as modeled in the Pythia MCEG. Another approach is the analysis of particle distributions in momentum space. This study does not require a precise knowledge of the top-quark flight direction as in the angular analysis. Furthermore, for the momentum spectra there are predictions based on the MLLA which we have explored previously for c- and b-quark jets in  $e^+e^-$  annihilation [6], also in comparison with Pythia8 MCEG [28]. For a stable top-quark the analysis could proceed in the same way and there are well-defined expectations on the effect of the heavy quark mass in the process  $e^+e^- \rightarrow t\bar{t} + X$  for the parton momentum distribution from the primary  $t\bar{t}$  color dipole radiation.

In the realistic case of an unstable top-quark, there are two additional features to be considered. Firstly, because of the decay of the top-quark  $t \rightarrow bW$ , we have an additional source of radiation from the color dipoles  $\widehat{tb}$  and  $\widehat{t\bar{b}}$  in the top-quark direction, which has to be separated. Secondly, there is a modification of the soft-gluon emission dependent on the finite width  $\Gamma_t$ . This effect will be discussed later in Sec. V as a correction and our analysis here is based on the PYTHIA 8.3 MCEG in its default version without this effect included.

The momentum distributions are studied using the variable  $\xi = \ln 1/x_p$  with the fractional momentum  $x_p = 2p/W$  at energy  $W = \sqrt{s}$  in the c.m.s. In  $e^+e^-$  annihilation we also refer to the fragmentation function

$$\bar{D}(\xi, W) = \frac{1}{2} \frac{1}{\sigma_{tot}} \frac{d\sigma^{e^+e^-}}{d\xi}(\xi, W) \quad (12)$$

with the particle density distribution  $d\sigma/d\xi$  in both hemispheres and the total production rate for the given event sample  $\sigma_{tot}$  and  $\bar{D}(\xi, W) = xD(\xi, W)$  with the inclusive distribution  $D(x, W)$  for one jet. In this section we refer to the  $\xi$ -spectra as  $2\bar{D}$  for both hemispheres for consistency with previous works.

The study of angular distributions in the last section has revealed that for angles  $|X_b| > 0.5$  between top- and b-quark the circular radiation around the top direction, often with discernible dead cone, becomes visible. In order to minimize the influence of the radiation from b-quarks we calculate the momentum spectra of the particles from the decays of the unstable top-quarks from the partons or hadrons with  $X_{p,h} > 0$  if the b-quark is moving along the negative  $X$ -axis and multiply the result by the factor 2. This configuration for the b-quark is obtained after appropriate rotation of the event around the top quark direction.

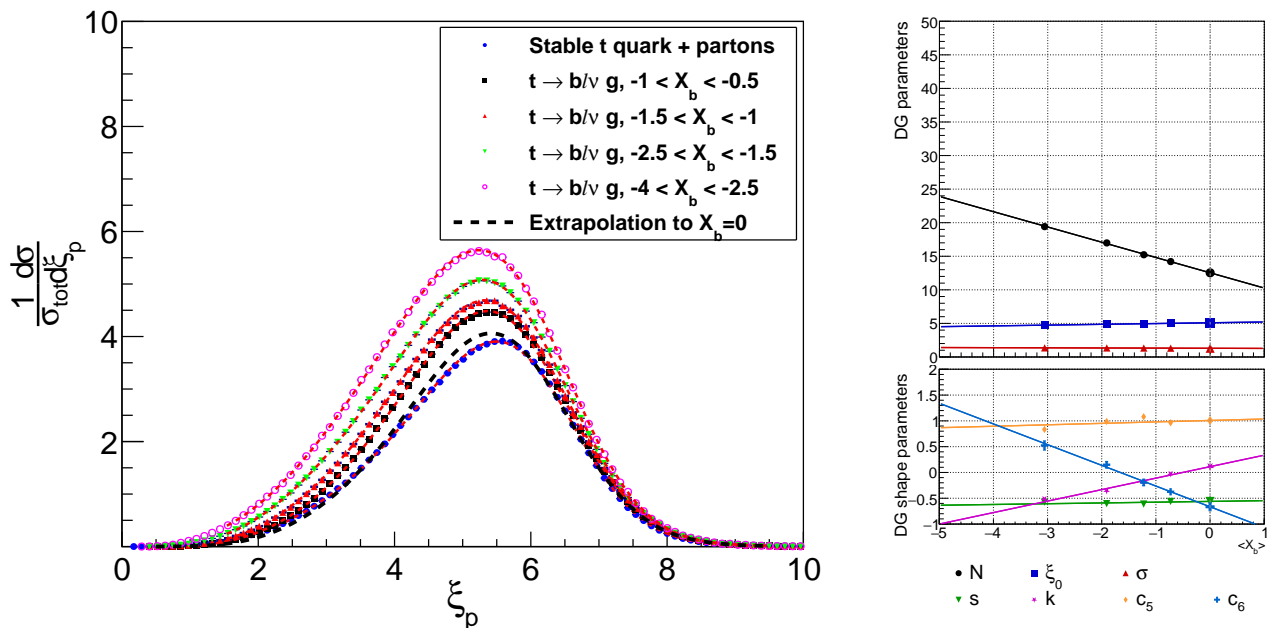


FIG. 9. Distribution of partons from top-quark decays over the momentum variable  $\xi_p = \ln(W/2p)$  at c.m.s. energy  $W = 1000$  GeV for different intervals in the decay angle  $X_b$  of the b-quark from top decay together with fits to the Distorted Gaussian (DG) distribution of  $O(z^6)$ . The dashed curve represents the extrapolation to forward direction  $X_b = 0$  in comparison with the  $\xi$ -distribution of the stable top quark (bottom line). The  $\xi$ -distributions are determined from the hemisphere away from the b-quark ( $X > 0$ ) and are multiplied by a factor 2; normalization of spectra to  $2\bar{D}(\xi, W)$  in Eq. (12); right panel: moment parameters of DG-distribution with fit to linear dependence on b-quark decay angle  $X_b$  and extrapolation to the results at  $X_b = 0$ .

At first, our aim is to reconstruct the  $\xi$ -distribution for the unstable top quark after the contribution of the  $\hat{t}\hat{b}$  dipole radiation is removed from the top-quark fragmentation region. As a test of this procedure we compare the result for partons with the  $\xi$ -distribution obtained for the stable top quark. This is the distribution which is used in the MLLA test for the relation between spectra for primary massive quarks with the ones for primary light quarks.

To this end we determine the  $\xi$ -distributions for different intervals of the b-quark decay angle  $X_b$  and extrapolate these distributions to the top quark direction  $X_b = 0$ . In this limit the radiation from the  $\hat{t}\hat{b}$  dipole is expected to vanish at high energies as discussed in the Sec. II, Eq. (6). The  $\xi$ -distributions of partons for different angular intervals of  $X_b$  are shown in Fig. 9. The maxima of these distributions are seen to decrease with decreasing  $|X_b|$ . The extrapolation of these  $\xi$ -distributions towards  $X_b \rightarrow 0$  is performed by fitting the distributions to a distorted Gaussian expansion, and to extrapolate the moment parameters. This representation is known to be well suited to fit the  $\xi$ -distributions [29]. The well known representation up to 4<sup>th</sup> order in  $z = (\xi - \xi_0)/\sigma$  fits the  $\xi$ -distributions for  $\xi \gtrsim 3$  only, therefore we added two more terms to fit the full  $\xi$ -region considered, see Appendix B. The moments are shown in the right panel of Fig. 9, and it is observed, that the data are well fitted to a linear dependence on  $X_b$ . From the extrapolated values at  $X_b = 0$  the corresponding  $\xi$ -distribution is reconstructed and is also shown in Fig. 9 as the dashed curve.

The same procedure is also applied to the  $\xi$ -spectra of hadrons which are selected from the right side hemisphere  $X_h > 0$  of the scatter plots in the lower panels of Fig. 18. In Fig. 10 we show the results of the fits to the  $\xi$ -distributions by the distorted Gaussian representation. The corresponding seven Gaussian moment parameters are again well fitted by a linear function, and in this way the extrapolated moments at  $X_B = 0$  and the extrapolated  $\xi$ -distribution can be obtained as in case of partons. This result from extrapolation represents the  $\xi$ -distribution for hadrons from top-quark decays with contributions from the  $\hat{t}\hat{b}$  dipole subtracted and is shown in Fig. 10 as dashed line.

For numerical values of the moment parameters, see Tab. II. There is a larger  $\chi^2$ -value for the lowest value of the b-quark angle  $X_b$  which we relate to the influence from the b-quark radiation into the right hemisphere  $X > 0$  close to top-quark direction. As a function of the b-quark angle  $X_b$  the main variation of the  $\xi$  distributions in Figs. 9 and 10 comes from the normalization while the shape varies only slightly. This is reflected in the behaviour of the moment parameters, where the strongest variation occurs in the multiplicity parameter  $N$  whereas the variation in

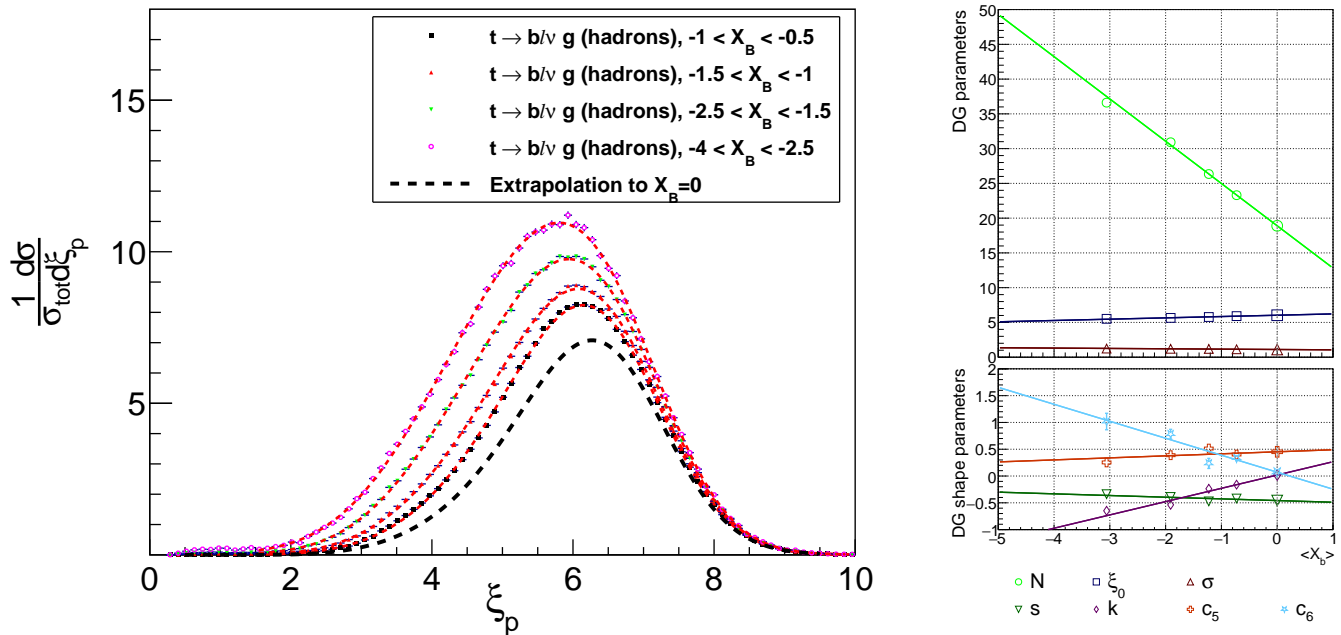


FIG. 10. Distribution over  $\xi = \ln(1/x_p)$  as in Fig. 9 but for hadrons. The  $\xi$ -distributions are shown for different intervals of the decay angle  $X_B$  of the b-quark from top decay, the dashed line represents their extrapolation towards the  $\xi$ -distribution at  $X_b = 0$  with the  $\hat{t}\hat{b}$  dipole radiation removed; right panel: moment parameters of DG distribution and linear fits to  $X_B$  dependence with extrapolation to  $X_B = 0$

Bin	$\langle X_b \rangle_{\text{part}}$	$\langle X_B \rangle_{\text{had}}$	Level	$N$	$\xi_0$	$\sigma$	$s$	$k$	$c_5$	$c_6$	$\chi^2/\text{ndf}$
1	-0.728	-0.728	partons	14.2	5.01	1.30	-0.561	-0.025	0.964	-0.374	5.83
			hadrons	23.3	5.90	1.13	-0.420	-0.161	0.401	0.333	10.1
2	-1.22	-1.22	partons	15.2	4.92	1.32	-0.612	-0.196	1.07	-0.194	3.65
			hadrons	26.3	5.77	1.19	-0.473	-0.237	0.512	0.235	3.39
3	-1.90	-1.91	partons	16.9	4.84	1.34	-0.604	-0.354	0.988	0.149	2.08
			hadrons	30.9	5.64	1.20	-0.390	-0.537	0.388	0.781	1.95
4	-3.05	-3.05	partons	19.4	4.77	1.35	-0.575	-0.512	0.834	0.522	1.78
			hadrons	36.6	5.51	1.24	-0.339	-0.648	0.253	1.01	1.24

TABLE II. Fit parameters of the Distorted Gaussian distribution of  $O(z^6)$  for the  $\xi$ -distributions of unstable top decays at parton and hadron level in four  $\langle X_b \rangle$  bins;  $\chi^2/\text{ndf}$  indicates fit quality.

the second and third moments is relatively small and the higher four moments are numerically small. This behaviour reflects the property of the distributions in leading order  $\alpha_s$  to factorize in energy  $\omega$  and angle  $\Theta_g$ , see Eq. (2), so the  $\xi$ -distribution in this approximation is independent of the angle  $X_b$ .

In Fig. 9 the extrapolated  $\xi$ -distribution for partons, the dashed line, is also compared with the control curve from the stable top-quark (bottom line). The same comparison is also shown in Fig. 11 in more detail. This is our main test for the success of our extrapolation method. The extrapolation removes the contribution from the  $\hat{t}\hat{b}$  dipole (the  $|B_1|^2$  contribution in Eq. (2)) and the  $|A|^2$  contribution for the stable top quark remains. There is a good agreement within about 5% near the maximum and below 12% for  $\xi \gtrsim 3$  within the variation of about 50% within the full extrapolation range. This indicates that the contributions from the  $\hat{t}\hat{b}$  dipole are effectively removed and we consider the remaining difference as a systematic error of the method.

A comparison of the hadron spectra with the stable top-quark as a check is not possible as there are no hadronic final states with the stable top hadron to be removed. We therefore rely on the successful extrapolation procedure for partons. A comparison between the moments for partons and hadrons shows that the main difference is in the larger multiplicity in an event for hadrons which is expected from hadronization. The behaviour and size of the other parameters is quite similar. A remarkable feature is the linearity in the dependences on angle  $X_b$ . This dependence

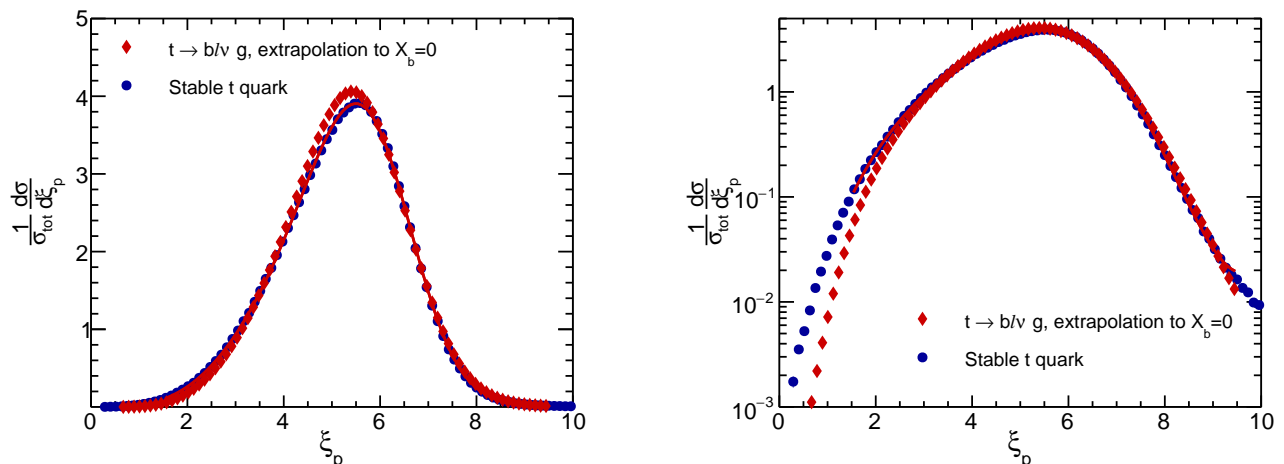


FIG. 11. Distribution over  $\xi_p = \ln(1/x_p)$  of partons as in Fig. 9 after extrapolation to forward decay angle  $X_b = 0$  of b-quark to remove the  $\hat{t}\hat{b}$  dipole radiation, in comparison with  $\xi$ -distribution for stable top-quark as consistency check, based on fits to Distorted Gaussian.

appears at the level of the parton evolution as is indicated from the behaviour of parton and hadron spectra for  $X > 0$  in the right panels of Figs. 7 and 19, while the dependence of the gluon spectrum on this angle is rather weak and it is expected to depend quadratically on the decay angle for small angles according to Eq. (5). The result obtained on the top-quark fragmentation distribution will now be compared with the MLLA expectations from the dead cone effect.

### B. Expectations for momentum spectra within the Modified Leading Log Approximation of QCD

The dead cone effect in heavy quark jets has first been established for the total multiplicities of light particles within the MLLA of perturbative QCD [1–4]. A corresponding relation for particle momentum spectra is not yet available in MLLA at the same rigor, but an equation for the inclusive  $x$ -spectra has been suggested which reproduces the equation for total multiplicities after integration over  $x$  and avoids a negative fragmentation function. This MLLA expectation has been reported in [2] and can be written in the  $\xi$  variable as

$$\bar{D}_Q(\xi, W) = \bar{D}_q(\xi, W) - \bar{D}_q(\xi - \xi_Q, \sqrt{e}m_Q) \quad (13)$$

with  $\xi_Q = \ln(1/\langle x_Q \rangle)$  for heavy quark  $Q$ . This equation relates the momentum distribution in the heavy quark jet at energy  $W$  to the one in the light quark  $q$  jet at the same energy after subtraction of the distribution at the reduced scale  $W_0 = \sqrt{e}m_Q$ . This equation has been found to be rather well supported by experimental data on  $c$ - and  $b$ -quark jets in the central  $\xi_p$  region for momenta  $p \gtrsim \Lambda_{QCD}$  [6]. For the top-quark we derive the numerical value for  $\xi_t$  from the top-quark energy distribution obtained in the Pythia 8.3 MCEG and obtain a rather small shift value  $\xi_t$

$$\langle x_t \rangle = 0.92, \quad \xi_t = 0.083 \quad \text{at } W = 1000 \text{ GeV}. \quad (14)$$

There are no experimental data available yet on these fragmentation functions to test Eq. (13). In the following we investigate how such a test could be performed using results obtained by Pythia 8.3. In addition we compare with the analytical QCD predictions in MLLA for the  $\bar{D}$  fragmentation-functions involved [2]. In the application of Eq. (13) we generate the distributions on the r.h.s. of Eq. (13) and derive the prediction for the heavy quark distribution on the l.h.s. which thereafter we will compare with the results obtained in the last subsection on the unstable top-quark. The elements for this prediction are shown in Fig. 12. The subtraction of the two distributions for light quarks at scales  $W$  and  $W_0$  yield the prediction (red triangles) with the strong suppression at small  $\xi$ .

We also show the results on the analytical calculations of the  $\xi$ -spectra in the MLLA of QCD, called “Limiting Spectrum” [30], for the two energies  $W$  and  $W_0$ . These functions are defined in terms of two parameters, the QCD scale  $\Lambda_{QCD}$  and the normalization  $K$ . In the derivation of the “Limiting Spectrum” it is assumed that the partonic branching process proceeds down to a hadronic cutoff  $Q_0 = \Lambda_{QCD}$  and this result can be compared directly to the

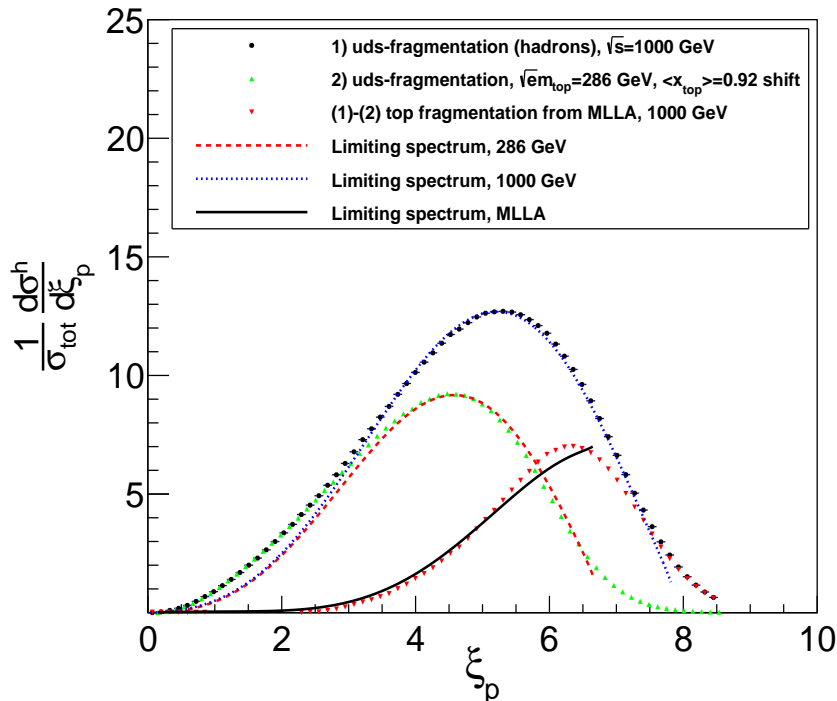


FIG. 12. Prediction for  $\xi_p$ -distributions in top quark fragmentation from MLLA of QCD for the hadrons shown as red triangle according to Eq. (13) using as input the  $\xi$ -distributions of light uds-quarks at energies  $W = 1000$  GeV and  $W_0 = 286$  GeV from Pythia 8.3 MCEG. Also shown are the results from the “limiting spectrum” of MLLA as curves.

spectrum of hadrons in accordance with the Local Parton Hadron Duality (LPHD) hypothesis [31, 32]. In order to obtain a good fit to the Pythia 8.3 data we adjusted the parameters slightly in comparison to our previous applications in [6], see Table III. This small variation of parameters reflects higher order perturbative contributions necessary for this large energy interval which are included in Pythia MCEG.

TABLE III.  $\mathcal{K}$  and  $\Lambda_{\text{QCD}}$  values for the relevant energy scales.

$\sqrt{s}$ (GeV)	$\Lambda_{\text{QCD}}$ (MeV)	$\mathcal{K}$
91.2	175	1.33
286	175	1.15
1000	200	1.105

A remarkable feature is the prediction of a strong suppression of particle production in the heavy quark jet at small  $\xi$  as compared to the light quark jet which reflects the dead cone effect for the heavy mass. On the other hand, at large  $\xi$  both distributions approach each other as the soft particles are emitted in a universal way independent of the quark mass.

### C. Test of MLLA predictions for top quark fragmentation

Finally we compare the results obtained from the angular extrapolation on the top quark fragmentation into hadrons in subsection IV A with the MLLA predictions. This is shown in Fig. 13.

The reconstructed distribution comes close to the distribution expected from the MLLA prediction (red triangles in Fig. 13) in a large region for  $\xi > 3$  to within about 15%. A failure of the MLLA approximation at the very small  $\xi$ -values (high momenta) should not be surprising as this approximation is developed for the bulk of particles with lower energies.

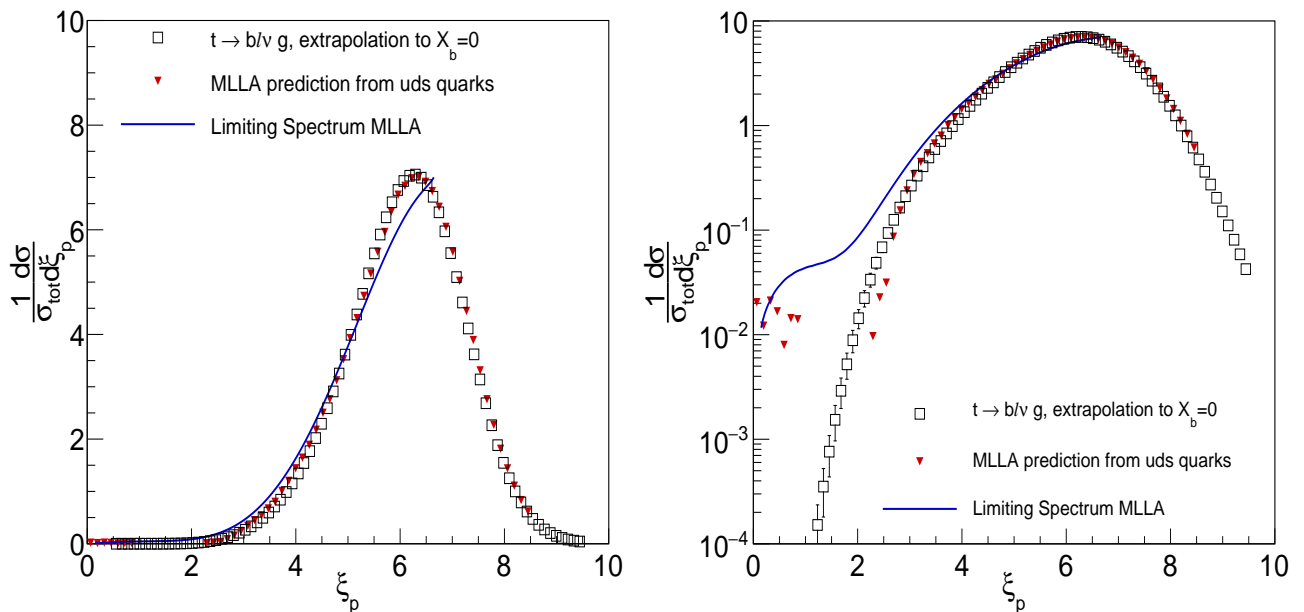


FIG. 13.  $\xi_p$ -distributions of hadrons for top fragmentation obtained by extrapolation to  $X_b = 0$  in comparison with the MLLA expectation from  $\xi_p$ -distributions from light quarks according to Eq. (13). Also shown the approximate formulae of the “Limiting Spectrum”, the same in Log scale in the right panel.

The main result of the study concerns the strong suppression of energetic particles with high energy and its understanding within QCD in terms of a simple connection with spectra from primary light quarks near the energies of the collision  $W$  and of the heavy quark mass  $m_Q$ . The ratio of the expected top quark fragmentation function to the light quark fragmentation function at  $W = 1000$  GeV for hadrons is shown in Fig. 14. It approaches 1 at large  $\xi$  for the soft particles and decreases down for fast particles at  $\xi \sim 2$  by a factor of  $\sim 100$ , again with a good agreement between t-quark fragmentation and MLLA prediction from light quark fragmentation.

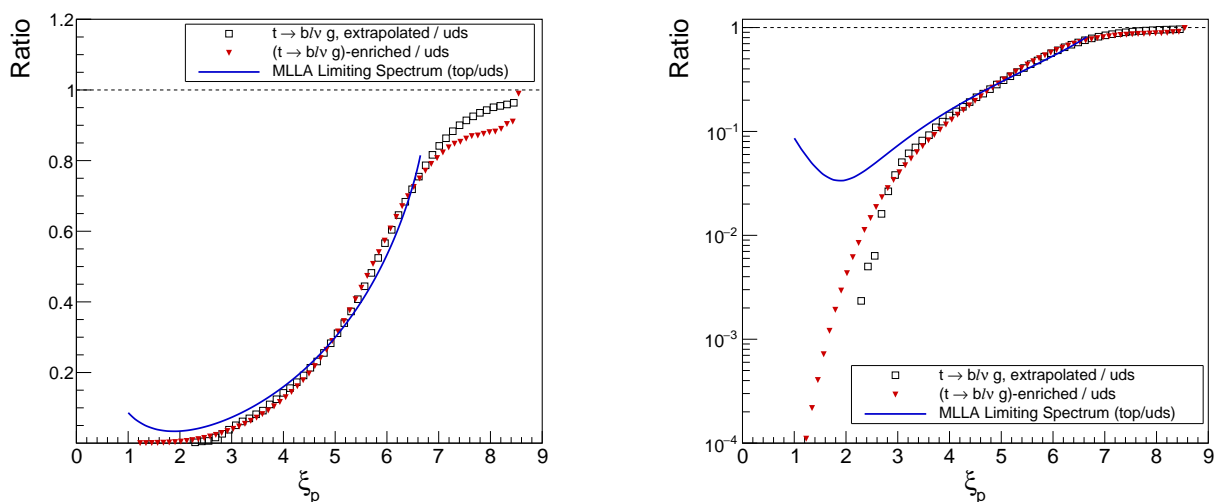


FIG. 14. Ratio of the top-quark fragmentation functions as in Fig. 13 over the fragmentation function for the primary light uds quarks showing the strong suppression of top quark fragmentation at small  $\xi$  or large momenta by a factor of about 100, also shown is the MLLA prediction using Limiting spectrum functions (full curve).

## V. MODIFICATIONS OF PARTICLE SPECTRA DUE TO FINITE WIDTH OF TOP QUARK

In our discussion so far we have assumed that production and decay of the top quark are separated by a large time interval and therefore there is no interference between the radiation emitted before and after decay. This corresponds to the default version of the Pythia 8 MCEG. Recently finite width effects in resonance decays have been included in parton showers in an “interleaved” treatment [33] based on the Vincia shower framework [34]. In this approach the parton branching process at low intrinsic  $p_T \lesssim \Gamma_t$  is modified and a suppression of final state particles with energies around the width  $\Gamma_t$  by a small amount is obtained. We investigate the consequences of this approach which is available in Pythia 8.3 with flag `TimeShower:recoilStrategyRF`.

In this way we obtain the modification of the  $\xi$ -spectra due to the finite top quark width shown in Fig. 15. This modification yields a small reduction in the rate of  $\lesssim 5\%$  at  $\xi \sim 5.8$ , the value corresponding to  $\xi \sim \ln(500 \text{ GeV}/\Gamma_t)$ , while there is no change below  $\xi \sim 3$  and a small increase at very large  $\xi$ , as also observed in [35]. The data show the result for the inclusive  $\xi$ -distribution, additional cuts did not produce major significant changes. The predicted effect is below the systematic errors coming from the subtraction of  $t\bar{b}$ -dipole radiation and is therefore not detectable within our analysis of momentum spectra.

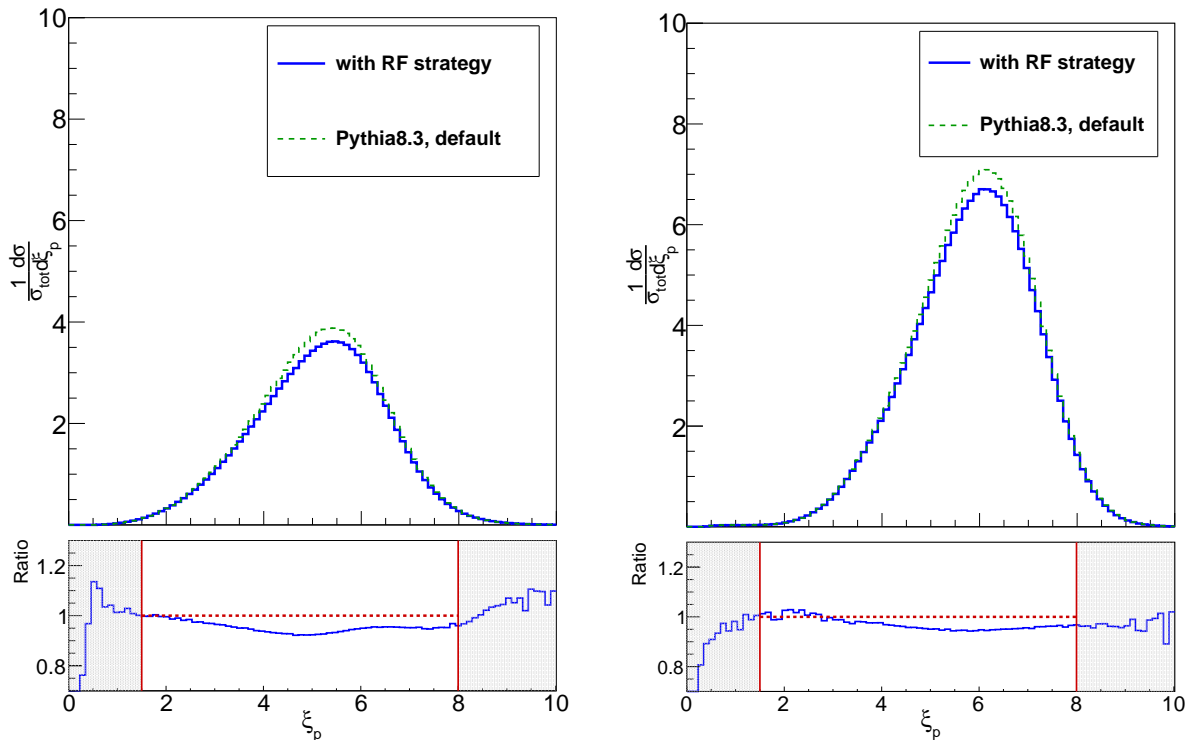


FIG. 15.  $\xi$ -distribution of partons (left panel), hadrons (right panel) with and without finite width correction according to the interleaved RF strategy of Pythia 8.3.

## VI. APPLICATIONS TO $pp$ COLLISIONS

So far we have discussed top-quark production in the reaction  $e^+e^- \rightarrow t\bar{t} + X$  which is most easily formulated theoretically and explored in the experimental analysis. There we considered the hadronic final state in the hemisphere of the produced top-quark. Unfortunately the related measurements will not become available for some time, if ever. Therefore, we will discuss in this section, how our results can be checked by measurements feasible at the Large Hadron Collider. The ATLAS and CMS collaborations have published data on  $t\bar{t}$  collisions at the LHC obtained with triggers on  $e^\pm, \mu^\pm$  from  $W$  decay or on purely hadronic jets. Cross sections have been measured for the top quark

transverse momentum up to  $p_T < 1000$  GeV and rapidity within  $|y| < 2.5$ , also the top mass  $m_t$  and  $\alpha_s$  have been determined, for results obtained at 13 TeV see e.g. Refs. [36–39].

In the application of our results to  $pp$ -collisions we have to consider top quark jets with associated particles in a cone around the top quark direction of half opening angle  $\Theta_{jet}$  isolated from the rest of the  $pp$  environment, in particular separated from the underlying event and pile-up collisions. Measurements of momentum or  $\xi$ -distributions of charged particles in high  $p_T$ -jet production by the CDF-collaboration at the Fermilab Tevatron  $p\bar{p}$  collider describe correction methods [40]. Pile-up mitigation at the LHC is effective for charged particles by associating them to the primary vertex of the hard interaction. Pile-up collisions have primary vertices separated along the beam direction and this can be measured well by the semiconductor based vertex detectors of the experiments.

In our study of the dead cone, the opening angle  $\Theta_{jet}$  should be chosen larger than the expected dead cone angle  $\Theta_0 = m_t/E_t$ . Looking at Fig. 3 an angular size of  $|X|, |Y| < R_X$  with  $R_X = 2 - 3$  appears appropriate, that corresponds to a jet opening angle  $\Theta_{jet} = (2 - 3) \Theta_0 \approx 40^\circ - 60^\circ$  at a jet energy of  $E_t = 500$  GeV as we had chosen above for  $e^+e^-$  annihilation. At the LHC the production of “fat jets” with jet radius  $R = R_X \Theta_0 > 1$  corresponding to  $\Theta_{jet} > 57^\circ$  has been discussed e.g. in [10, 41].

The top jet direction is estimated as the sum over the momenta of the leptons from the  $W$  decay and the hadrons inside the large jet cone  $\Theta_{jet}$ . The further analysis should in principle proceed in analogy to the case of  $e^+e^-$  annihilation. The particles inside the cone are analysed by the jet finder, two jets are formed and they are classified as b-jet and gluon jet. A plot of the masses as in Fig. 5 will identify events along the vertical stripe with preferred top quark radiation  $t \rightarrow tg$  to be selected. The  $\xi$ -distribution of hadrons is then constructed from the hadrons in the hemisphere opposite to the b-quark jet, and the final  $\xi$ -distribution is found by extrapolation in the distance  $R_{X,b}$  of the relative angle between b-quark jet and top-quark direction.

The test of the MLLA expectation for the  $\xi$ -distribution of particles emitted from the top quark follows as in Eq. (13) but the energy scale has to be redefined according to the reduced jet opening angle [17, 30, 40]

$$W \rightarrow 2E_{jet} \sin \Theta_{jet} , \quad (15)$$

so we rewrite Eq. (13) for the inclusive spectrum in a single jet with energy  $E_{jet}$  at half opening angle  $\Theta_{jet}$

$$\bar{D}_Q(\xi, E_{jet}; \Theta_{jet}) = \bar{D}_q(\xi, E_{jet} \sin(\Theta_{jet})) - \bar{D}_q(\xi - \xi_Q, \sqrt{em}q) \quad (16)$$

If the opening angle  $\Theta_{jet}$  is reduced the distribution of particles with high momenta or small  $\xi$  which dominate at small angle remain unchanged but the production of low momentum particles at large  $\xi$  is suppressed. Clearly, for  $\Theta_{jet} \rightarrow \Theta_0$  the particle density vanishes in the approximation of Eq. (16) and thus the relation can only be meaningful for sufficiently large jet angles. The dependence of characteristics of the  $\xi$ -spectra on the jet angle as in Eq. (15) has been experimentally confirmed by the CDF collaboration [40].

The MLLA equation Eq. (16) relates the  $\xi$ -distribution in top quark production to the ones in light quark production at different energy scales. These distributions at the required higher energies in the TeV range are not yet measured. These could be obtained at the LHC e.g. from reactions with subprocesses such as  $gq \rightarrow \gamma q$  involving light quarks  $q$  or by relying on the QCD based MCEG.

The accuracy of Eqs. (13), (16) is expected to increase with rising energy and thereby with decreasing dead cone angle  $\Theta_0$ . This can also be seen by comparing our present result for top production with our previous result on  $b$ -quarks [6]. While our analysis for  $b$ -quarks at  $W = 90$  GeV had an angle  $\Theta_0 \approx 6^\circ$  and has shown agreement with MLLA expectations in a large kinematic region within  $\lesssim 10\%$  we found above for the case of stable top quark with  $\Theta_0 \approx 20^\circ$  a discrepancy of  $\lesssim 15\%$ . The discrepancy for limited opening angle  $\Theta_{jet}$  is expected to be larger and thus it is desirable to use the highest possible top jet momenta available with reasonable statistics in the LHC data.

## VII. CONCLUSIONS

We have studied the feasibility of observing the forward emission of particles in a high energy top-quark jet with dead cone which is characteristic for the elementary QCD process of gluon emission from a massive quark. Our analysis is based on the application of the Pythia 8.3 MCEG for the generation of events in the reaction  $e^+e^- \rightarrow t\bar{t} + X$  at  $\sqrt{s} = 1$  TeV.

At first, we studied the angular distribution of particles around the top-quark direction which are bundled into the b-quark jet and the primary gluon jet. In case of a stable top-quark one finds the emission of gluons in a forward jet, but with suppression in the direction of the t-quark as expected in perturbative QCD and already observed in c- and b-quark production (“dead cone”). A new phenomenon in top-quark production is the additional radiation generated by the b-quark from the top-quark decay which partially obscures the dead cone phenomenon. In leading order in

$\alpha_s$  the additional radiation into the top-quark hemisphere comes from the  $\hat{t}\hat{b}$  dipole which is superimposed to the  $\hat{t}\hat{t}$  dipole for the stable top-quark production with dead cone and is characterized by the following properties:

- (a) the gluons emitted in direction of the b-quark are strongly limited in angle to half the top-quark hemisphere by “angular ordering”, as can be observed in the individual MC events and also in the 2-dim scatter plots;
- (b) The gluons emitted from the  $\hat{t}\hat{b}$  dipole in the t-quark direction fill partially the forward dead cone generated by the  $\hat{t}\hat{t}$  dipole and radiate into the hemisphere opposite to the b-quark; its density increases with increasing b-quark decay angle against naive expectation. The effect is enlarged for the parton or hadron final state.

In view of these results the desired momentum distribution of partons in the top-quark jet is then constructed from the partons in the half hemisphere opposite to the b-quark to avoid contributions from  $\hat{t}\hat{b}$  dipole radiation. Momentum distributions of partons are determined for different b-quark decay angles  $\Theta_b$  and they are extrapolated to angle  $\Theta_b = 0$  where the contribution of the  $\hat{t}\hat{b}$  dipole radiation is expected to vanish. The resulting distribution for partons compares well with the corresponding distribution for the stable top-quark to within 5 – 15% which we consider as successful test of the method. The same procedure yields the momentum distribution of hadrons for the stable top-quark.

This fragmentation function for the top-quark is found in MCEG to be suppressed for large momenta or small  $\xi = \ln(2p/\sqrt{s})$ , at  $\xi \sim 3$  by a factor 1/100, in comparison to the momentum distribution for corresponding light quark jets. We also found that the MLLA prediction which relates the top-quark fragmentation function to the light quark fragmentation functions at c.m.s. energies  $\sqrt{s}$  and  $m_t$  is well satisfied by our analysis based on Pythia 8.3 within these uncertainties around 10%. This is in support of the construction of the jet final state within perturbative QCD, in particular of the role of angular ordering within the evolution process at the large intrinsic scale of  $m_t \sim 172$  GeV. Furthermore, we investigated the influence of the finite top-quark width on the particle spectra within a special option of the Pythia MCEG. The effect exists for low momenta, but it is too small to be reliably resolved given our systematic uncertainty.

Our analysis is performed for the forward hemisphere in the direction of the top-quark in  $e^+e^-$  annihilation. This type of analysis appears to be feasible also for high  $p_T$  top-quark production in pp collisions at the LHC, where the jet cone angle for detection of the top-quark jet and the influence from the underlying event and pile-up collisions have to be taken into account in the analysis.

### Appendix A: Angular distributions of partons and hadrons in top-quark jet

In this subsection we report on further studies of the angular structure of top-quark jets formed by partons and hadrons which evolve from the primary gluons. First we present in Fig. 16 the 2-dim  $(X, Y)$  distribution as in Fig. 3, but for partons. The central dead cone is partially filled but still visible. Also shown is the distribution in the angle  $\Theta^2/\Theta_0^2$  of the final partons themselves. This broadening of the distributions is expected from the convolution of two distributions. Therefore, the suppression near zero angle is weaker and the dead cone effect is reduced.

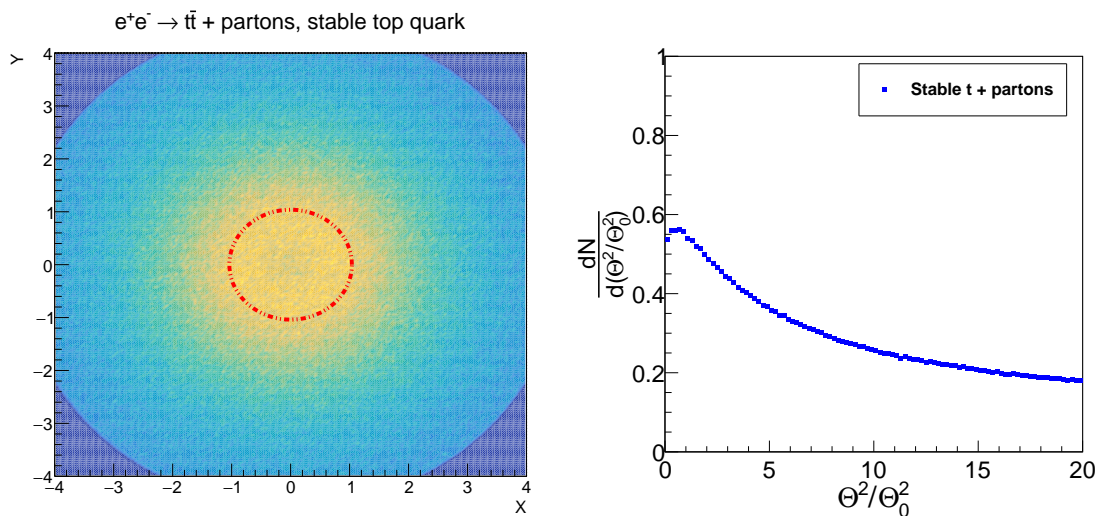


FIG. 16. Angular distribution of partons around the top-quark direction showing a suppression of density in the center as in Fig. 3 but of smaller magnitude and distribution in the rescaled opening angles  $\Theta/\Theta_0$  (top-quark excluded).

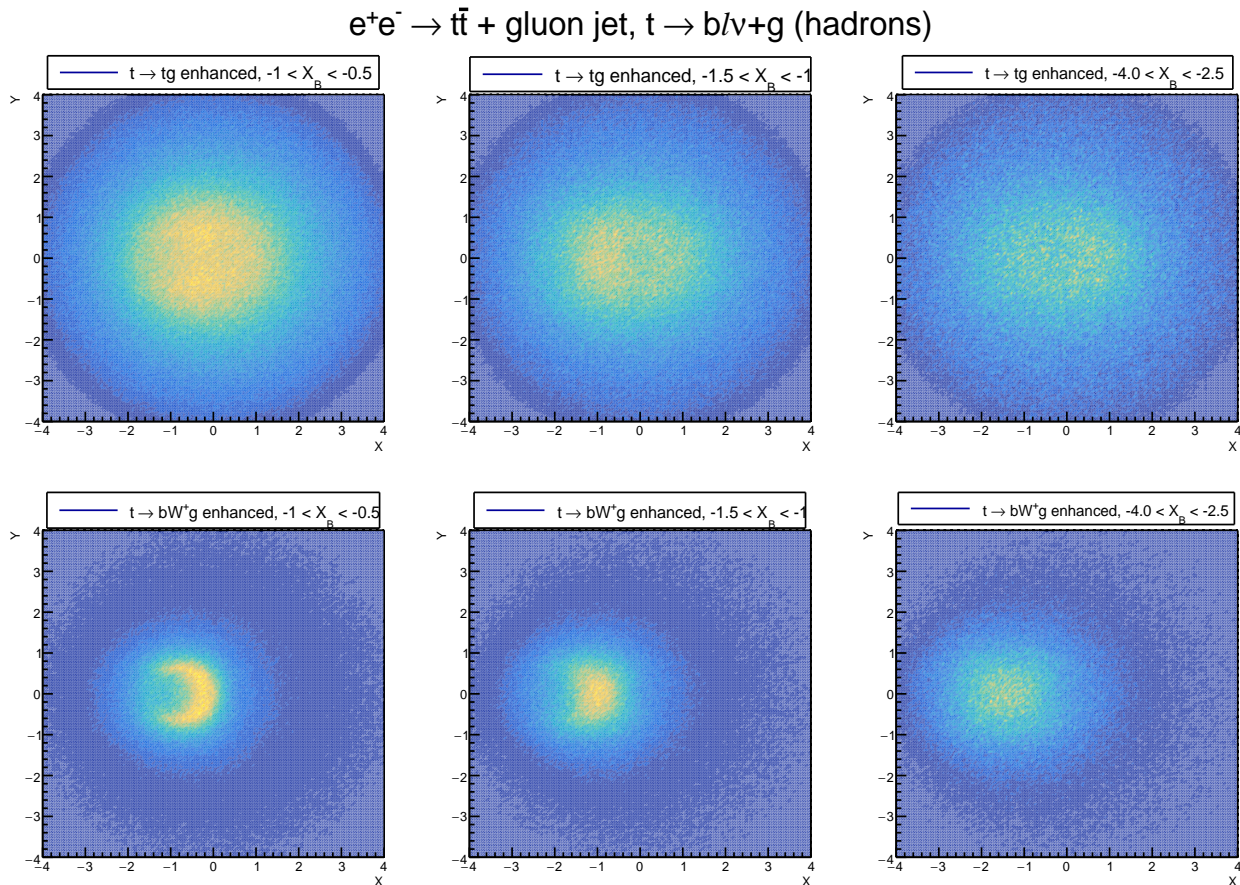


FIG. 17. Angular distributions as in Fig. 6 but for hadrons: gluon jets constructed from hadrons for events enhanced with top-quark gluon emission  $t \rightarrow tg$  for different angles of the B-jet  $X_B$  to the top quark (upper panels) and with gluon jets enhanced with top-quark decay  $t \rightarrow b\ell\nu + g$  (lower panels).

For the unstable top quark we have constructed the angular distribution of gluons also from the hadronic final state in a similar way as we did for partons in Fig. 6, i.e. we assigned the hadrons to two jets, the one with a B-hadron is chosen as b-jet, the other one as gluon jet. The  $(X, Y)$  angular distribution of these gluon jets constructed from hadrons are shown in Fig. 17, in the upper row for the vertical stripe in Fig. 5 (right panel) which enhances the process  $t \rightarrow tg$ . There is again evidence of the dead cone surrounded by a circular distribution of radius  $R_X \sim 1$ . The suppression of the b-jet signal inside the jet radius  $R = 0.2$  is only weakly visible here. This may indicate that the hadronization process in its MC realization yields a weaker collimation of gluons to their primary sources. On the other hand, for the angular distributions in the lower row with t-quark decays enhanced, the half moon-type jet signature clearly shows up as for partons.

Finally we also present the angular distributions of the final state partons and hadrons for events with dominating  $t \rightarrow tg$  process selected from the vertical stripes of Fig. 5. Their  $(X, Y)$  angular distributions are shown in Fig. 18 using the same selection criteria for the masses. Again, the two different components of b- and t-quark radiation around the two centers are clearly visible, the dead cone in the center in most cases is hardly visible. We also note, that at small b-quark angles  $X_b$  for hadrons (lower left panel) the b-quark radiation extends slightly into the positive hemisphere  $X > 0$  in a violation of angular ordering valid at parton level.

The distributions for gluon jets built from hadrons and for hadrons themselves along the central horizontal stripe in the  $(X, Y)$  scatter plot, in analogy to Fig. 7 for partons, are shown in Fig. 19. Here the same ordering trends for the different b-quark angles  $X_b$  at positive  $X$  are observed as in the figure for partons. The gluon jets are seen to be widely independent of the b-quark angle for  $X_g > 0$  which indicates a reduced influence of the  $t\bar{b}$  dipole.

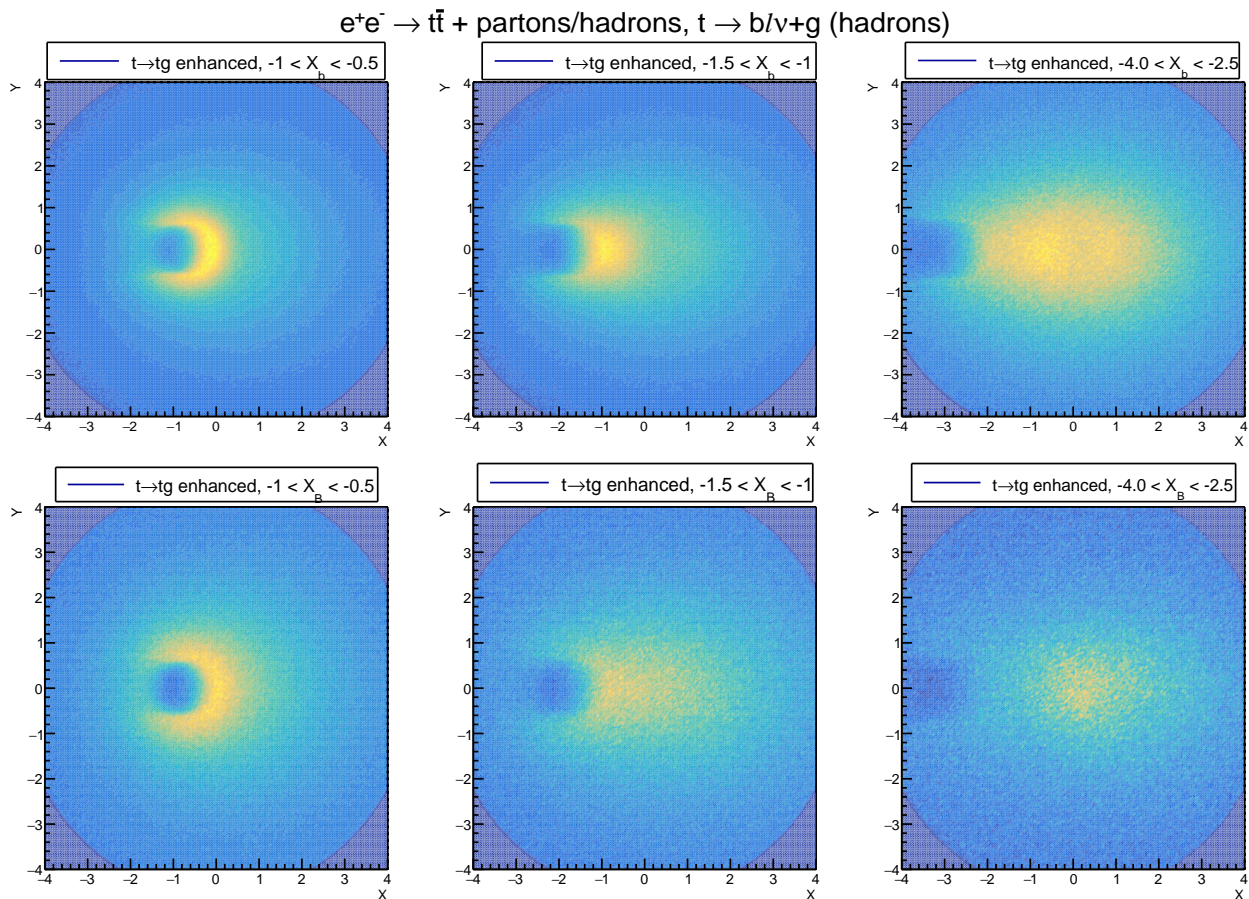


FIG. 18. Distributions over  $(X, Y)$  angles of partons (upper row) and hadrons (lower row) for different angular regions of the b-quark jet  $X_b$  or B-hadron jet  $X_B$ , all for events with top gluon emission  $t \rightarrow tb$  enhanced (vertical stripe in Fig. 5).

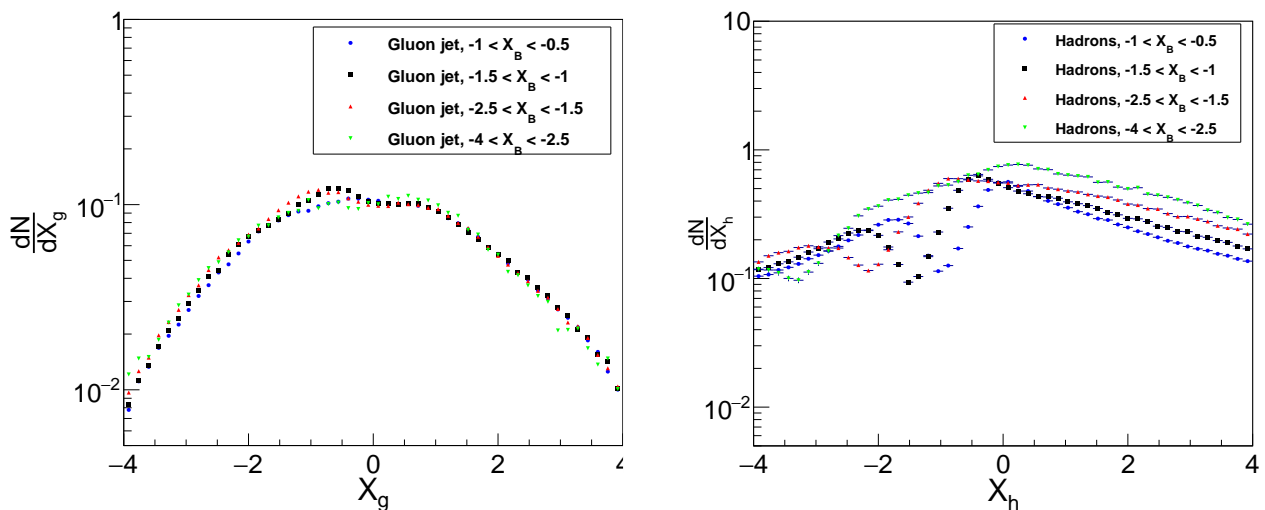


FIG. 19. Distributions as in Fig. 7 but for hadron final states: gluon jets over the angles  $X_g$  and hadrons over  $X_h$  along central stripe through  $(X, Y)$  scatter plots in Fig. 17, upper row and in Fig. 18, lower row. The dependence of the spectra in the hemisphere  $X_h > 0$  on the B-jet decay angle  $X_B$  is similar to the one for partons and reflects the  $\hat{t}\bar{b}$  dipole contribution.

## Appendix B: Distorted Gaussian with $z^5$ and $z^6$ Corrections

We define the dimensionless scaling variable

$$z \equiv \frac{\xi - \xi_0}{\sigma}, \quad (\text{B1})$$

where  $\xi_0$  and  $\sigma$  denote the position of the maximum and the width of the distribution, respectively. The full distorted Gaussian distribution is given by

$$D(\xi) = \frac{N}{\sigma\sqrt{2\pi}} \exp \left[ F \left( \frac{\xi - \xi_0}{\sigma} \right) \right], \quad (\text{B2})$$

where the exponent  $F(z)$  is written as (see [29] for a review)

$$F(z) = \frac{k}{8} - \frac{s}{2}z - \frac{1}{4}(2+k)z^2 + \frac{s}{6}z^3 + \frac{k}{24}z^4 + \frac{c_5}{120}z^5 + \frac{c_6}{720}z^6. \quad (\text{B3})$$

Here:

- $N$  is the overall normalization, corresponding to the particle multiplicity in the Gaussian limit;
- $\xi_0$  is the position of the maximum of the distribution;
- $\sigma$  is the width parameter;
- $s$  controls the skewness of the distribution;
- $k$  controls the kurtosis;
- $c_5$  and  $c_6$  parameterize higher order shape deformations.

The different powers of  $z$  in Eq. (B3) have distinct qualitative effects:

- odd powers  $z$  and  $z^3$  (controlled by  $s$ ) generate left right asymmetry;
- even powers  $z^2$  and  $z^4$  (controlled by  $k$ ) modify the peak sharpness and tail structure;
- the  $z^5$  term introduces a higher order asymmetric deformation ( $c_5$ );
- the  $z^6$  term modifies the symmetric tails at higher order ( $c_6$ ).

The parameter  $N$  sets the overall normalization (multiplicity in the Gaussian limit), while  $s, k, c_5, c_6$  control deviations from a pure Gaussian shape. An illustration of the role of the various parameters on the shape of the  $\xi$ -distribution is presented in Fig. 20.

### Normalization

Changing variables  $\xi \rightarrow z = (\xi - \xi_0)/\sigma$ , the integral becomes

$$\int_{-\infty}^{+\infty} D(\xi) d\xi = \frac{N}{\sqrt{2\pi}} \int_{-\infty}^{+\infty} e^{F(z)} dz. \quad (\text{B4})$$

We now separate the exponent into a standard Gaussian part and a deformation,

$$F(z) = -\frac{1}{2}z^2 + \varepsilon(z) \quad (\text{B5})$$

$$\varepsilon(z) = \frac{k}{8} - \frac{s}{2}z - \frac{k}{4}z^2 + \frac{s}{6}z^3 + \frac{k}{24}z^4 + \frac{c_5}{120}z^5 + \frac{c_6}{720}z^6. \quad (\text{B6})$$

It is convenient to introduce the Gaussian-weighted average

$$\langle g(z) \rangle_G \equiv \frac{1}{\sqrt{2\pi}} \int_{-\infty}^{+\infty} g(z) e^{-z^2/2} dz. \quad (\text{B7})$$

With this definition, the exact normalization reads

$$\int_{-\infty}^{+\infty} D(\xi) d\xi = N \langle e^{\varepsilon(z)} \rangle_G. \quad (\text{B8})$$

In the pure Gaussian limit ( $\varepsilon = 0$ ), one has  $\langle 1 \rangle_G = 1$  and therefore  $\int D(\xi) d\xi = N$ .

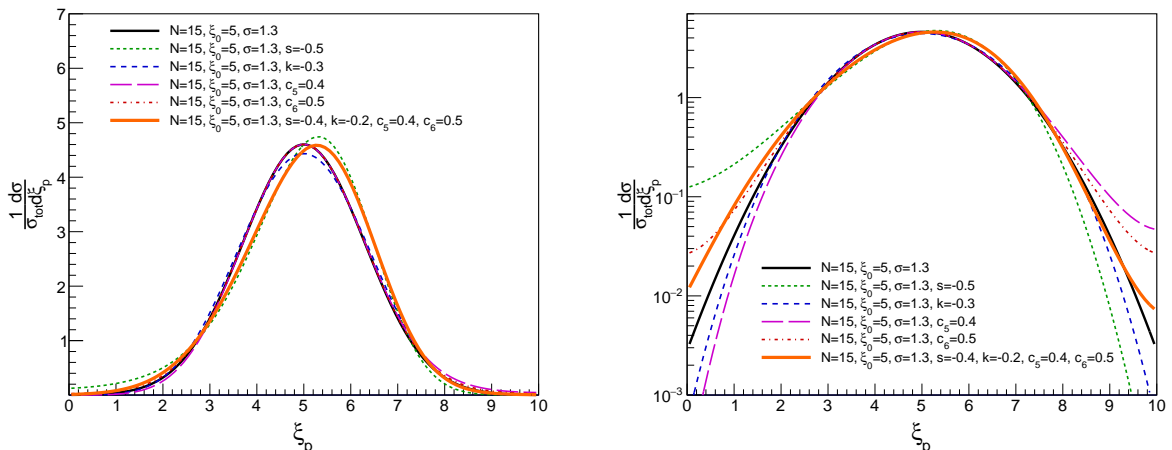


FIG. 20. Illustration of the distorted Gaussian parametrization of the logarithmic momentum distribution  $D(\xi)$ . The black curve shows the pure Gaussian limit ( $s = k = c_5 = c_6 = 0$ ). Each additional curve isolates the effect of a single deformation parameter switched on individually: skewness ( $s \neq 0$ , green), kurtosis ( $k \neq 0$ , blue), fifth order deformation ( $c_5 \neq 0$ , magenta), and sixth order tail correction ( $c_6 \neq 0$ , red). The numerical values are chosen for illustration only, in order to make the qualitative effect of each term clearly visible; they are not intended as fitted values.

### Small-deformation expansion

For small deviations from Gaussianity we expand

$$e^{\varepsilon(z)} \simeq 1 + \varepsilon(z), \quad (\text{B9})$$

so that

$$\int_{-\infty}^{+\infty} D(\xi) d\xi \simeq N (1 + \langle \varepsilon(z) \rangle_G). \quad (\text{B10})$$

Using the standard Gaussian moments with respect to  $\langle \cdot \rangle_G$ ,

$$\langle z \rangle_G = 0, \quad \langle z^2 \rangle_G = 1, \quad \langle z^3 \rangle_G = 0, \quad \langle z^4 \rangle_G = 3, \quad \langle z^5 \rangle_G = 0, \quad \langle z^6 \rangle_G = 15,$$

one finds, to linear order in the deformation parameters,

$$\langle \varepsilon(z) \rangle_G = \frac{k}{8} - \frac{k}{4} + \frac{k}{8} + \frac{15}{720} c_6 = \frac{c_6}{48}. \quad (\text{B11})$$

Therefore, to leading order,

$$\int_{-\infty}^{+\infty} D(\xi) d\xi = N \left( 1 + \frac{c_6}{48} + \mathcal{O}(s^2, k^2, c_5^2, c_6^2) \right). \quad (\text{B12})$$

In particular, if  $s = k = c_5 = c_6 = 0$ , the DG distribution reduces to a Gaussian and the integral equals  $N$  exactly.

### Appendix C: Kinematics

We define the three momenta for top-quark, parton and  $e^-$  beam as

$$\mathbf{p}^t = (p_x^t, p_y^t, p_z^t), \quad \mathbf{p} = (p_x, p_y, p_z), \quad \mathbf{p}^{e^-} = (p_x^{e^-}, p_y^{e^-}, p_z^{e^-}). \quad (\text{C1})$$

The vector normal to the plane spanned by the top quark and the parton is

$$\mathbf{p}_\perp^{t,p} = \mathbf{p}^t \times \mathbf{p} \quad (\text{C2})$$

and the vector normal to the plane spanned by the top quark and the electron

$$\mathbf{p}_{\perp}^{t,e^{-}} = \mathbf{p}^t \times \mathbf{p}^{e^{-}}. \quad (\text{C3})$$

The azimuthal angle  $\phi$  between the two planes is defined through

$$\cos \phi = \frac{\mathbf{p}_{\perp}^{t,p} \cdot \mathbf{p}_{\perp}^{t,e^{-}}}{|\mathbf{p}_{\perp}^{t,p}| |\mathbf{p}_{\perp}^{t,e^{-}}|}. \quad (\text{C4})$$

and its orientation is fixed by the sign of

$$s = (\mathbf{p}_{\perp}^{t,p} \times \mathbf{p}_{\perp}^{t,e^{-}}) \cdot \mathbf{p}^t, \quad (\text{C5})$$

such that

$$\phi = \begin{cases} \arccos(\cos \phi), & s > 0, \\ 2\pi - \arccos(\cos \phi), & s < 0. \end{cases}$$

The polar angle  $\Theta$  between the parton and the top quark momentum is given by

$$\Theta = \arccos\left(\frac{\mathbf{p}^t \cdot \mathbf{p}}{|\mathbf{p}^t| |\mathbf{p}|}\right). \quad (\text{C6})$$

Finally, this yields the coordinates in the plane perpendicular to the top-quark direction used for our angular scatter plots

$$X = (\Theta/\Theta_0) \cos \phi, \quad Y = (\Theta/\Theta_0) \sin \phi,$$

such that  $R_X^2 = X^2 + Y^2 = (\Theta^2/\Theta_0^2)$ . In our presentation of angular scatter plots we present the distributions after rotation around the top-quark direction, so that the B hadron points into the negative X direction. This is achieved by replacing all azimuthal coordinates  $\phi$  by

$$\phi' = \phi - \phi_B - \pi. \quad (\text{C7})$$

- 
- [1] Y. L. Dokshitzer, V. A. Khoze, and S. I. Troian, Particle spectra in light and heavy quark jets, *J. Phys. G* **17**, 1481 (1991).
- [2] Y. L. Dokshitzer, V. A. Khoze, and S. I. Troian, On specific QCD properties of heavy quark fragmentation ('dead cone'), *J. Phys. G* **17**, 1602 (1991).
- [3] B. A. Schumm, Y. L. Dokshitzer, V. A. Khoze, and D. S. Koetke, MLLA and the average charged multiplicity of events containing heavy quarks in  $e^+e^-$  annihilation, *Phys. Rev. Lett.* **69**, 3025 (1992).
- [4] Y. L. Dokshitzer, F. Fabbri, V. A. Khoze, and W. Ochs, Multiplicity difference between heavy and light quark jets revisited, *Eur. Phys. J. C* **45**, 387 (2006), arXiv:hep-ph/0508074.
- [5] S. Acharya *et al.* (ALICE Collaboration), Direct observation of the dead-cone effect in quantum chromodynamics, *Nature* **605**, 440 (2022), erratum: *Nature* **607** (2022) no.7920, E22, arXiv:2106.05713 [nucl-ex].
- [6] S. Kluth, W. Ochs, and R. Perez Ramos, Observation of the dead cone effect in charm and bottom quark jets and its QCD explanation, *Phys. Rev. D* **107**, 094039 (2023), arXiv:2303.13343 [hep-ph].
- [7] S. Navas *et al.* (Particle Data Group), Review of particle physics, *Phys. Rev. D* **110**, 030001 (2024).
- [8] G. Aad *et al.* (ATLAS Collaboration), Measurement of the top quark mass with the template method in the  $t\bar{t} \rightarrow$  lepton+jets channel using atlas data, *Eur. Phys. J. C* **72**, 2046 (2012), arXiv:1203.5755 [hep-ex].
- [9] A. Tumasyan *et al.* (CMS Collaboration), Measurement of the top quark mass using a profile likelihood approach with the lepton+jets final states in proton-proton collisions at  $\sqrt{s} = 13$  TeV, *Eur. Phys. J. C* **83**, 963 (2023), arXiv:2302.01967 [hep-ex].
- [10] G. Aad *et al.* (ATLAS Collaboration), Measurement of the top quark mass with the ATLAS detector using  $t\bar{t}$  events with a high transverse momentum top quark, *Phys. Lett. B* **867**, 139608 (2025), arXiv:2502.18216 [hep-ex].
- [11] G. V. Jikia, Measuring the heavy top quark width by soft gluon radiation in  $e^+e^- \rightarrow t\bar{t}$ , *Phys. Lett. B* **257**, 196 (1991).
- [12] V. A. Khoze, W. J. Stirling, and L. H. Orr, Soft gluon radiation in  $e^+e^- \rightarrow t\bar{t}$ , *Nucl. Phys. B* **378**, 413 (1992).
- [13] F. Maltoni, M. Selvaggi, and J. Thaler, Exposing the dead cone effect with jet substructure techniques, *Phys. Rev. D* **94**, 054015 (2016), arXiv:1606.03449 [hep-ph].

- [14] C. Bierlich, S. Chakraborty, N. Desai, L. Gellersen, I. Helenius, P. Ilten, L. Lönnblad, S. Mrenna, S. Prestel, C. T. Preuss, T. Sjöstrand, P. Skands, M. Uthmeim, and R. Verheyen, A comprehensive guide to the physics and usage of PYTHIA 8.3, *SciPost Phys. Codebases*, **8** (2022), arXiv:2203.11601 [hep-ph].
- [15] T. Sjostrand, S. Ask, J. R. Christiansen, R. Corke, N. Desai, P. Ilten, S. Mrenna, S. Prestel, C. O. Rasmussen, and P. Z. Skands, An Introduction to PYTHIA 8.2, *Comput. Phys. Commun.* **191**, 159 (2015), arXiv:1410.3012 [hep-ph].
- [16] B. Andersson, G. Gustafson, G. Ingelman, and T. Sjöstrand, Parton Fragmentation and String Dynamics, *Phys. Rept.* **97**, 31 (1983).
- [17] Y. L. Dokshitzer, V. A. Khoze, A. H. Mueller, and S. I. Troyan, *Basics of Perturbative QCD* (Editions Frontières, Gif-sur-Yvette, France, 1991).
- [18] B. I. Ermolaev and V. S. Fadin, Log-log asymptotic form of exclusive cross-sections in quantum chromodynamics, *JETP Lett.* **33**, 269 (1981).
- [19] A. H. Mueller, On the multiplicity of hadrons in QCD jets, *Phys. Lett. B* **104**, 161 (1981).
- [20] R. K. Ellis, W. J. Stirling, and B. R. Webber, *QCD and Collider Physics* (Cambridge University Press, Cambridge, 2011) DOI: 10.1017/CBO9780511628788.
- [21] P. Martín-Ramiro and J. M. Moreno, Improving  $t\bar{t}$  reconstruction in the dilepton channel at future lepton colliders, arXiv:2003.12320 [hep-ph] (2020).
- [22] T. Behnke *et al.*, The international linear collider technical design report – volume 4: Detectors (2013), arXiv:1306.6329 [physics.ins-det].
- [23] M. Cacciari, G. P. Salam, and G. Soyez, Fastjet user manual, *Eur. Phys. J. C* **72**, 1896 (2012), arXiv:1111.6097 [hep-ph].
- [24] M. Cacciari and G. P. Salam, Dispelling the  $n(3)$  myth for the k.t jet-finder, *Phys. Lett. B* **641**, 57 (2006), arXiv:hep-ph/0512210 [hep-ph].
- [25] G. Aad *et al.* (ATLAS Collaboration), Performance of  $b$ -jet identification in the ATLAS experiment, *JINST* **11** (04), P04008, arXiv:1512.01094 [hep-ex].
- [26] G. Aad *et al.* (ATLAS Collaboration), Performance of jet substructure techniques for large- $R$  jets in proton–proton collisions at  $\sqrt{s} = 7$  TeV using the ATLAS detector, *JHEP* **09**, 076, arXiv:1306.4945 [hep-ex].
- [27] S. Chatrchyan *et al.* (CMS Collaboration), Identification of  $b$ -quark jets with the CMS experiment, *JINST* **8** (04), P04013, arXiv:1211.4462 [hep-ex].
- [28] S. Kluth, W. Ochs, and R. Perez-Ramos, Dead cone effect in charm and bottom quark jets, *Nucl. Part. Phys. Proc.* **343**, 75 (2024), arXiv:2309.01708 [hep-ph].
- [29] C. P. Fong and B. R. Webber, One and two particle distributions at small  $x$  in QCD jets, *Nucl. Phys. B* **355**, 54 (1991).
- [30] Y. L. Dokshitzer, V. A. Khoze, and S. I. Troian, Phenomenology of the particle spectra in QCD jets in a modified leading logarithmic approximation, *Z. Phys. C* **55**, 107 (1992).
- [31] Y. I. Azimov, Y. L. Dokshitzer, V. A. Khoze, and S. I. Troyan, Similarity of Parton and Hadron Spectra in QCD Jets, *Z. Phys. C* **27**, 65 (1985).
- [32] Y. I. Azimov, Y. L. Dokshitzer, V. A. Khoze, and S. I. Troyan, Humpbacked QCD Plateau in Hadron Spectra, *Z. Phys. C* **31**, 213 (1986).
- [33] H. Brooks, P. Skands, and R. Verheyen, Interleaved resonance decays and electroweak radiation in the Vincia parton shower, *SciPost Phys.* **12**, 101 (2022), arXiv:2108.10786 [hep-ph].
- [34] H. Brooks and P. Skands, Coherent showers in decays of colored resonances, *Phys. Rev. D* **100**, 076006 (2019), arXiv:1907.08980 [hep-ph].
- [35] S. Dittmaier and M. Reyer, Electroweak splitting functions in the standard model and beyond, arXiv:2507.06568 [hep-ph] (2025), arXiv:2507.06568 [hep-ph].
- [36] M. Aaboud *et al.* (ATLAS Collaboration), Measurements of top-quark pair differential cross-sections in the lepton+jets channel in  $pp$  collisions at  $\sqrt{s} = 13$  TeV using the ATLAS detector, *JHEP* **11**, 191, arXiv:1708.00727 [hep-ex].
- [37] V. Khachatryan *et al.* (CMS Collaboration), Measurement of differential cross sections for top quark pair production using the lepton+jets final state in proton–proton collisions at  $\sqrt{s} = 13$  TeV, *Phys. Rev. D* **95**, 092001 (2017), arXiv:1610.04191 [hep-ex].
- [38] A. M. Sirunyan *et al.* (CMS Collaboration), Measurement of the  $t\bar{t}$  production cross section, the top quark mass, and the strong coupling constant using dilepton events in  $pp$  collisions at  $\sqrt{s} = 13$  TeV, *Eur. Phys. J. C* **79**, 368 (2019), arXiv:1812.10505 [hep-ex].
- [39] G. Aad *et al.* (ATLAS Collaboration), Measurements of top-quark pair single- and double-differential cross-sections in the all-hadronic channel in  $pp$  collisions at  $\sqrt{s} = 13$  TeV using the ATLAS detector, *JHEP* **01**, 033, arXiv:2006.09274 [hep-ex].
- [40] D. Acosta *et al.* (CDF Collaboration), Momentum distribution of charged particles in jets in dijet events in  $p\bar{p}$  collisions at  $\sqrt{s} = 1.8$  TeV and comparisons to perturbative QCD predictions, *Phys. Rev. D* **68**, 012003 (2003).
- [41] A. Tumasyan *et al.* (CMS), Measurement of the differential  $t\bar{t}$  production cross section as a function of the jet mass and extraction of the top quark mass in hadronic decays of boosted top quarks, *Eur. Phys. J. C* **83**, 560 (2023), arXiv:2211.01456 [hep-ex].